Title

Biophysical transport model suggests climate variability determines distribution of Walleye Pollock early life stages in the eastern Bering Sea through effects on spawning

Authors

Petrik, Colleen M
Duffy-Anderson, Janet T
Mueter, Franz
et al.

Publication Date

2015-11-01

DOI

10.1016/j.pocean.2014.06.004

Peer reviewed

Biophysical transport model suggests climate variability determines distribution of Walleye Pollock early life stages in the Eastern Bering Sea through effects on spawning

Colleen M. Petrik[1,*,a], Janet T. Duffy-Anderson[2], Franz Mueter[1], Katherine Hedstrom[3], and Enrique N. Curchitser[4]

[1]University of Alaska Fairbanks, School of Fisheries and Ocean Sciences, 17101 Point Lena Loop Rd., Juneau, AK 99801, USA

[2]Alaska Fisheries Science Center, NOAA NMFS, 7600 Sand Point Way NE, Seattle, WA 98115, USA

[3]University of Alaska Fairbanks, Arctic Region Supercomputing Center, 105 West Ridge Research Bldg., P.O. Box 756020, Fairbanks, AK 99775, USA

[4]Department of Environmental Sciences and Institute of Marine and Coastal Sciences, Rutgers University, 14 College Farm Rd., New Brunswick, NJ 08901, USA

*Corresponding author. Email: cpetrik@ucsc.edu. Tel.: 508-274-8620

[a]Present affiliation and address: UC Santa Cruz, Institute of Marine Sciences, NOAA NMFS SWFSC, 110 Shaffer Rd., Santa Cruz, CA 95060, USA

ABSTRACT

The eastern Bering Sea recently experienced an anomalously warm period followed by an anomalously cold period. These periods varied with respect to sea ice extent, water temperature, wind patterns, and ocean circulation. The distributions of Walleye Pollock early life stages also differed between periods, with larval stages found further eastward on the shelf in warm years. Statistical analyses indicated that these spatial distributions were more closely related to temperature than to other covariates, though a mechanism has not been identified. The objective of this study was to determine if variable transport could be driving the observed differences in pollock distributions. An individual-based model of pollock early life stages was developed by coupling a hydrodynamic model to a particle-tracking model with biology and behavior. Simulation experiments were performed with the model to investigate the effects of wind on transport, ice presence on time of spawning, and water temperature on location of spawning. This modeling approach benefited from the ability to individually test mechanisms to

quantitatively assess the impact of each on the distribution of pollock. Neither interannual variability in advection nor advances or delays in spawning time could adequately represent the observed differences in distribution between warm and cold years. Changes to spawning areas, particularly spatial contractions of spawning areas in cold years, resulted in modeled distributions that were most similar to observations. The location of spawning pollock in reference to cross-shelf circulation patterns is important in determining the distribution of eggs and larvae, warranting further study on the relationship between spawning adults and the physical environment. The different distributions of pollock early life stages between warm and cold years may ultimately affect recruitment by influencing the spatial overlap of pollock juveniles with prey and predators.

Keywords: biophysical model; climate change; larval fish; *Gadus chalcogrammus*; *Theragra chalcogramma*

1. INTRODUCTION

The eastern Bering Sea shelf is one of the most biologically productive marine ecosystems in the world with marine resources that are integral to the culture and diet of native Alaskans and that comprise roughly 50% of the US commercial fish harvest. The continental shelf extends approximately 500 km westward from the Alaskan mainland coast to the Aleutian Basin shelfbreak and 1000 km northward from the Alaska Peninsula to the Bering Strait. The shelf can be divided into three regions based on bathymetry: inner shelf (<50 m), middle shelf (50-100 m), and outer shelf (>100 m; Coachman 1986). The inner shelf is weakly stratified and influenced by freshwater runoff, while the middle and outer shelves are strongly stratified (Coachman 1986). A large and highly variable portion of the shelf is ice-covered during winter, cooling the entire water column and resulting in a bottom layer of very cold water (the "cold pool") over much of the middle shelf that can persist through the summer. Offshore, the Bering Slope Current (Figure 1) transports nutrient-rich waters along the slope to the northwest, replenishing nutrients on the shelf through cross-shelf exchanges associated with eddies (Mizobata et al. 2008), intrusions of water through canyons (Stabeno et al. 2008), and wind-forced cross-shelf flows (Stabeno et al. 2001, Danielson et al. 2011b). Mean circulation over the shelf is dominated by the Alaska Coastal Current, which is a seasonal current that flows roughly

63 parallel to the 50-m isobath northeast along the Alaska Peninsula, around Bristol Bay, and
64 continues to the northwest off of mainland Alaska towards the Bering Strait (Figure 1). Cross-
65 shelf and along-shelf flows provide important pathways for the planktonic stages of many
66 species that spawn on the outer shelf or slope to reach suitable nursery areas (Lanksbury et al.
67 2007, Wespestad et al. 2000, Wilderbuer et al. 2013).
68 Walleye Pollock (*Gadus chalcogrammus*; hereafter pollock) is an ecologically and
69 commercially important gadid in the eastern Bering Sea, supporting one of the largest single-
70 species fisheries in the world. Adults are semi-demersal and occur primarily in regions 50-300 m
71 deep (J. Duffy-Anderson pers. comm.). Females are iterative spawners with up to 10 batches of
72 eggs per female per year (J. Duffy-Anderson pers. comm.). Pollock show fidelity to at least two
73 spawning sites over the southeastern Bering Sea shelf (Figure 1). Spawning begins nearshore
74 north of Unimak Island in March and April and later near the Pribilof Islands from April through
75 August (Jung et al. 2006, Bacheler et al. 2010). Egg production from these two locations is
76 highest in April or May (Bacheler et al. 2010). Eggs can be found as deep as 300 m, but the
77 center of the vertical distribution is < 30 m (Smart et al. 2012). Depending upon water
78 temperature, embryos hatch 18 to 34 days after fertilization and yolksac larvae are 4.6 to 5.7 mm
79 standard length (SL) at hatch (Blood 2002). Larvae develop in the upper 100 m of the water
80 column and the depth of maximum abundance shifts deeper with age (Smart et al. 2013). Depth
81 differences are related to flexion, which occurs between 10 and 17 mm SL (Matarese et al.
82 1989), after which larval swimming ability increases. Pollock transition from larva to pelagic
83 juvenile when they are 30-40 mm SL (Matarese et al. 1989) and recruit into the fishery at age-3
84 to age-4 (Ianelli et al. 2012a).
85 The eastern Bering Sea recently experienced a prolonged warm period (2001-2005),
86 followed by a prolonged cold period (2007-2012; Stabeno et al. 2012). During colder than
87 average years, winter ice extends farther south and offshore, creating a more extensive cold pool
88 that influences the distribution (Mueter & Litzow 2008, Barbeaux 2012, Ianelli et al. 2012a) and
89 potentially the spawning ecology of pollock and other demersal fishes. The timing and location
90 of pollock spawning affect the initial distribution of eggs, while their subsequent advection is a
91 function of prevailing atmospheric and hydrographic conditions. Therefore both the initial
92 distribution and advective forcing vary from year-to-year due to climatic variability. For
93 example, strong northward flow and/or weaker cross-shelf flow have been observed at a

hydrographic mooring over the middle shelf during the recent warm period compared to recent cold years that had strong westward flow (Stabeno et al. 2012), which could affect the dispersal of pelagic early life stages (ELS). Modeling results suggest generally enhanced on-shelf transport when winds blow predominantly from the southeast during winter (Danielson et al. 2011a). Such southeasterly winds coincided with warm temperatures from 2001 to 2005, while the following cold years were characterized by winds from the northwest. It has been speculated that these differences in advection influence the distributions of pollock ELS, whose centers are further inshore in warm years than cold years (Smart et al. 2012).

The observed variability in distribution could be the result of differences in physical transport as hypothesized, or they could be the result of biological responses to physical variation. Preliminary analysis of roe fishery harvest data and pollock fishery observer maturity data suggest that spawning extends further onshore in warm years (S. Barbeaux unpub. data) and the onset of spawning is delayed in time by as much as 40 d in cold years (Jung et al. 2006, Smart et al. 2012). Differences in water temperature could impact not only where adults spawn, but also the development rates of ELS.

Mechanisms behind the spatial differences have not been identified, and effects of climate variation on the dispersal of pollock ELS are poorly understood. The differences in winds and water currents between cold and warm years, and the relationship between temperature and pollock spatial distribution lead to our hypothesis that physical forcing mechanisms are responsible. To gain a clearer understanding of the forcing mechanisms that underlie observed spatial differences in pollock egg and larval distribution, we developed an individual-based model of pollock biology and behavior coupled to a hydrodynamic model. Our objective was to test the effects of atmospheric (wind), oceanographic (ice, water column temperature), and biological (time and location of spawning) conditions on the distribution, development, and transport of pollock eggs and larvae. Model results are used to elucidate the dominant physical mechanisms responsible for observed changes. We present a description of the coupled biophysical model, its validation with observations, and its use to evaluate mechanisms that determine the spatial distribution of propagules during warm and cold years.

2. METHODS

2.1 Physical model

We used an implementation of the Regional Ocean Modeling System (ROMS; Shchepetkin & McWilliams 2009) as the hydrodynamic model to force the Lagrangian particle-tracking model. ROMS is a free-surface, hydrostatic primitive equation ocean circulation model. It is a terrain-following, finite volume (Arakawa C-grid) model with the following advanced features: high-order, weakly dissipative algorithms for tracer advection; a unified treatment of surface and bottom boundary layers (e.g., K-Profile Parameterization; Large et al. 1994); atmosphere-ocean flux computations based on the ocean model prognostic variables using bulk-formulae. ROMS has been coupled to a sea-ice model (Budgell 2005) consisting of the elastic-viscous-plastic (EVP) rheology (Hunke & Dukowicz 1997) and the Mellor and Kantha (1989) thermodynamics. The sea ice code is fully explicit and implemented on the ROMS Arakawa C-grid and is therefore fully parallel, just as ROMS is. The model also includes frazil ice growth in the ocean being passed to the ice (Steele et al. 2004). It currently follows a single ice category, which provides accurate results in a marginal ice zone such as the Bering Sea. Large-scale climate signals are propagated to the regional domain through the model boundaries. This global-to-regional downscaling via open boundary conditions has several desirable features for the implementation of regional models: for multi-decadal integrations, climate signals project onto the high-resolution inner domains through boundary forcing; tidal forcing is naturally implemented on the domain open boundaries; for extensive integrations a tidal potential correction is applied to ensure proper tidal phasing (Curchitser et al. 2005, Danielson et al. 2011a).

We used the ROMS model for the northeast Pacific version 6 (NEP6), an update of version 5 (NEP5; Hermann et al. 2009, Danielson et al. 2011a). The NEP model domain extends from approximately 20 °N to 71 °N, reaching about 2250 km offshore from the North American west coast at a nominal horizontal resolution of 10 km and with 50 terrain-following vertical levels stretched towards the surface boundary. The grid (a rectangle in a Lambert Conical projection) is rotated relative to lines of constant longitude so as to minimize computations over land. The coupled ocean-sea ice model was integrated in hindcast mode for the period from 1994-2012. These hindcasts derived the surface forcing from the Modern Era Retrospective-Analysis for Research and Applications (MERRA; Rienecker et al. 2011), which consists of 3-hourly winds, air temperatures, sea level pressure, specific humidity, short-wave and downwelling long-wave radiation, precipitation, and daily albedo. The air-sea fluxes were

156 computed using bulk formulae (Large & Yeager 2009). Riverine inputs were implemented using
157 the Dai and Trenberth (2002) method as a surface fresh water flux. Boundary and initial
158 conditions for this domain were derived from the Simple Ocean Data Assimilation (SODA)
159 ocean reanalysis (Carton & Giese 2008) for the early years. Later years used boundary
160 conditions from global HYCOM assimilative product (HYCOM Ocean Prediction website). Key
161 model outputs have recently been validated against observations at relevant spatial and temporal
162 scales (Curchitser et al. 2010, Danielson et al. 2011a).
163 The output of the hindcast was saved as daily averages to force the offline particle-
164 tracking model, as described below. Specifically, the particle-tracking model used ROMS-
165 generated velocities, temperature, and mixed layer depth.
166
167 **2.2 Particle-tracking model**
168 *2.2.1 TRACMASS*
169 We implemented the individual-based model with the particle-tracking tool
170 TRACMASS. TRACMASS calculates Lagrangian trajectories from Eulerian velocity fields. The
171 coupling is offline, using stored output from general circulation model (GCM) simulations.
172 Offline coupling is less computationally expensive, thus it allows for more calculations of
173 trajectories in comparison with online coupling (simultaneously with the GCM). TRACMASS
174 accepts output from many GCMs, including ROMS. TRACMASS interpolates the GCM three-
175 dimensional grid to its own grid and solves the trajectory path through each grid cell with an
176 analytical solution of a differential equation, which depends on the velocities at the grid cell
177 walls. This novel scheme was originally developed by Döös (1995) and Blanke and Raynaud
178 (1997) for stationary velocity fields and further developed by de Vries and Döös (2001) for time-
179 dependent fields. With time-dependent fields it solves a linear interpolation of the velocity field
180 both in time and in space over each grid box, in contrast to the Runge-Kutta method where the
181 trajectories are iterated forward in time with short time steps. The TRACMASS code has been
182 further developed over the years and used in many atmospheric and oceanographic studies of
183 large global (e.g. Drijfhout et al. 2003) and regional scales (e.g. Engqvist et al. 2006).
184 The particle-tracking time step was one hour. We chose to use the turbulence subroutine
185 in TRACMASS to incorporate a sub-grid scale parameterization. This scheme adds a random
186 horizontal turbulent velocity to the horizontal velocity from ROMS to each trajectory and each

187 horizontal grid wall every time step (Döös & Engqvist 2007). The amplitude of the random
188 turbulent velocity is set to the same size as the ROMS velocity. We tested simulations of a small
189 cluster of particles with and without sub-grid turbulence. Including turbulence resulted in less
190 patchy distributions of ELSs, which were assumed to be more realistic, although fine-scale data
191 to evaluate this assumption are lacking. In addition to particle trajectories, TRACMASS
192 calculated surface light as a function of latitude, longitude, date, and time of day.
193
194 *2.2.2 Number of particles*
195 Often results from stochastic models are presented as the average of several repeated
196 simulations with the same initial and forcing conditions. For particle-tracking models, an
197 alternate method exists of releasing multiple particles at each time and location, each
198 representing one possible outcome of the simulation. The results of a rigorous particle-tracking
199 model should not change significantly between repeated simulations (Brickman et al. 2009). The
200 number of particles released at each time and location (number of simulation repetitions) was
201 determined by calculating the fraction of particles at four random locations downstream of the
202 initial start locations, and finding the minimum number of particles for which those fractions did
203 not change appreciably. Ten particles per 10 m depth increment per spawning location were
204 deemed appropriate for producing stable results.
205
206 **2.3 Observational data**
207 *2.3.1 Ichthyoplankton surveys*
208 Observational data from the Alaska Fisheries Science Center's Fisheries Oceanography
209 Coordinated Investigations (FOCI) surveys and Bering Ecosystem Study and Bering Sea
210 Integrated Ecosystem Research Project (BEST-BSIERP) cruises were used for model-data
211 comparisons. The specific cruise details are given in Smart et al. (2012). Observational data
212 included egg and larval samples collected with Bongo nets, Multiple Opening/Closing Net and
213 Environmental Sensing System (MOCNESS), Modified Bottom Trawls (MBTs), and Tucker
214 trawls. Larval stages were segregated by length: yolksac < 6 mm; 6 mm ≤ preflexion < 10 mm;
215 10 mm ≤ late < 40 mm (Matarese et al. 1989). Data from all four gear types were used to
216 characterize horizontal distributions, while only depth-stratified MOCNESS samples were used
217 for the vertical distributions since the other gear types did not provide enough vertical resolution.

218 Horizontal distributions were determined for each stage and for each available month and year
219 from 1995 to 2012, by aggregating all observations within a given month and year. To quantify
220 horizontal distributions, vertically integrated concentrations (number per 10 m^2) were computed
221 over the entire depth range sampled by depth-stratified tows (MOCNESS, MBT, Tucker) so that
222 they were comparable to non-stratified samples (Bongo). All available data sets from 1995 and
223 2007, years with the best spatial and temporal coverage, were used for model selection. Data
224 from all years (1995-2012), for the cruises listed in Smart et al. (2012), were aggregated by
225 warm and cold years for comparison between observed and modeled distributions in warm and
226 cold years.
227
228 *2.3.2 Spawning data*
229 Two different data sets were used to provide information on potential locations for
230 initializing particles as eggs in the model. The first data set was derived from collections of
231 female pollock for the roe fishery (S. Barbeaux unpub. data). These data included the day of
232 fishing, the centroid latitude and longitude of where the boat fished that day, and the amount of
233 roe of each quality caught that day for the years 2001-2006. The market quality of roe
234 deteriorates as the adults near spawning and is ranked as immature, mature, overmature, or other.
235 Hydrated, overmature roe is within a few days of spawning and of the worst quality (S. Barbeaux
236 pers. comm.). We used only presence and absence data of the hydrated roe as a proxy for
237 spawning times and locations.
238 The second data set consisted of maturity index classifications from the NOAA Fisheries
239 North Pacific groundfish observer program. These data were obtained on pollock fillet fishery
240 vessels from 2008-2012 and contained date, latitude, longitude, bottom depth, fishing depth, and
241 a maturity index for each fish. Observers classify the maturity level of a random subsample of
242 the catch using the maturity indices: immature, developing, pre-spawn, spawning, and spent. We
243 used only the dates and locations where female pollock in spawning condition were recorded as a
244 proxy for spawning times and locations.
245 These data were used together with available literature on dominant spawning areas
246 (Bacheler et al. 2010, Hinckley 1987) to infer generalized spawning distributions for warm and
247 cold years, respectively, as described below. We were unable to use annual observations on
248 spawning times and locations for model initialization because neither data set spanned the whole

time period of interest from 2000 to 2012. Furthermore, we chose not to combine the two data sets because they used data from different fisheries with different classification methods, of which one only included cold years and the other only warm years.

2.4 Biological model

2.4.1 Model parameterization

The literature on pollock ELS was reviewed to determine appropriate formulations for the growth and vertical behavior routines in the biological model. When available, data from the Bering Sea population was used in preference to data from the Gulf of Alaska.

2.4.1.1 Growth

Egg development was implemented as a temperature-dependent function parameterized from laboratory data for Bering Sea pollock eggs (Blood 2002). Time to hatch, $hatch_{hrs}$ (hr) (Figure 2a), was

$$hatch_{hrs} = 895.97 \cdot e^{-0.194 \cdot T},$$

with temperature, T, in °C. At each time step, an egg accumulated a fraction of the hatch time given the temperature. When the accumulated hatch time reached 1, the egg transitioned to the yolksac stage. Size at hatch was not related to incubation temperature in a laboratory study with Bering Sea eggs, thus yolksac larvae were initialized at a random hatch length drawn from a normal distribution with a mean of 5.125 mm SL and a standard deviation of 0.46 mm (Blood 2002).

Both a temperature-dependent and an age-dependent (temperature-independent) growth model were developed for larvae to allow for tests of the effect of temperature on growth and the resulting distributions of different ELS. The age-dependent routine was an empirical function for length, L_{larva} (mm), fit to otolith-estimated age of larvae collected in the Gulf of Alaska by Yoklavich and Bailey (1990) during summer 1987, a year with slightly above average temperature conditions (7-11˚C in the surface layer).

$$L_{larva} = L_{hatch} \cdot \exp(7.854 \cdot (1 - \exp(-0.004 \cdot age)))$$

where L_{hatch} is length at hatch (mm), and age is days post hatch (dph; Figure 2c solid line). The temperature-based growth model fitted growth rates from laboratory studies as a function of

temperature (Canino 1994 for yolksac, Porter & Bailey 2007 for feeding larvae). Yolksac larvae growth, g_y (mm d^{-1}; Figure 2b), was

$$g_y = 0.0686 \cdot \log(T) + 0.0594 .$$

Growth of feeding larvae (preflexion and late larvae), g_f (mm d^{-1}), was additively adjusted to account for differences in laboratory growth rates of larvae fed a natural assemblage of zooplankton vs. those fed *Artemia*. Growth (Figure 2b, 2c dotted lines) was calculated as

$$g_f = 0.0902 \cdot \log(T) - 0.0147 .$$

Larval length is only updated for nonnegative growth rates at temperatures above 1.17˚C, thereby preventing larvae from shrinking at lower temperatures.

2.4.1.2 Vertical behavior

Vertical behaviors were determined from depth-stratified observations of pollock ELS in the Bering Sea (Smart et al. 2013). Five different vertical behavior routines were developed and tested. They included: 1) passive (neutrally buoyant) individuals of all stages; 2) passive eggs and yolksac larvae, and preflexion and late larvae that move to the middle of the mixed layer; 3) all stages move to the middle of the mixed layer; 4) eggs, yolksac, and preflexion larvae move to the middle of the mixed layer, and late larvae make diel vertical migrations (DVMs) between 20 m during the day and 5 m during the night; 5) eggs and yolksac larvae move to the middle of the mixed layer, and preflexion and late larvae make DVMs. For DVM, day was defined as times when surface light was greater than zero. Swimming speed (w) was parameterized as:

$$w = w_{\max} \cdot (-\tanh(0.2 \cdot (z - z_{pref})))$$

where z is depth (m), z_{pref} (m) is the preferred depth (middle of the mixed layer or day-time/night-time preferred depths), and the maximum vertical swimming speed, w_{max} (m s^{-1}), is

$$w_{\max} = 0.5 \cdot L_{larva} \cdot 10^{-3} .$$

Swimming speeds of larval Atlantic Cod (*Gadus morhua*), a related gadid fish, range from 0.3-0.9 body lengths s^{-1} (Peck et al. 2006), thus a maximum speed of 0.5 body lengths s^{-1} was a conservative estimate for sustained swimming.

2.4.2 Model initialization

Spawning polygons were created by generalizing areas with fishery-based observations of adult pollock in spawning condition. Only the dominant spawning regions on the eastern Bering Sea shelf, as identified from the literature (Hinckley 1987, Bacheler et al. 2010), were considered. Spawning observations in regions deeper than 250 m were not used, as these are likely to consist of spawners from the Bogoslof Island population, which is considered to be a separate population from that over the eastern Bering Sea shelf (Ianelli et al. 2012b). Polygons were created for 2-week periods from the middle of January to the end of April for a total of seven periods (Figure 3; release dates Jan 15, Feb 1, Feb 15, Mar 1, Mar 15, Apr 1, Apr 15). These dates cover the spawning season and represent the iterative spawning of pollock, though at a lower frequency than the natural population. Spawning was initialized at all ROMS grid points within each spawning polygon. Spawning depths occurred every 10 m from surface to bottom at each grid point. Individuals were followed from spawning time until they reached 40 mm. At approximately 30-40 mm SL pollock larvae transition to pelagic juveniles with different growth rates and enhanced swimming abilities (Matarese et al. 1989), which were not represented within the model.

2.4.3 Model selection

Two years with the most spatially and temporally resolved observations (1995, 2007; both cold years) were used to choose the growth and vertical behavior routines to be implemented in all other simulations of the model. Ten different growth-behavior combinations (two growth functions, five vertical behaviors) were run for each year, for a total of 20 different simulations.

The observational data were used to calculate the average monthly concentration for each ELS in 0.25° x 0.25° grid cells over the eastern Bering Sea (-175°W to -160°W, 53°N to 61°N) for comparisons with model output aggregated at the same spatial scale. When multiple observations occurred within the same grid cell, the mean concentration was used. A grid cell without any observations was set to “missing”.

To account for uneven spatial coverage of samples among years and to reduce the impact of small-scale sampling variability resulting from patchiness and/or sampling errors, observed concentrations were spatially smoothed using a General Additive Modeling (GAM) approach. We modeled log-transformed concentrations of each ELS in each month as a smooth function of

latitude and longitude using a flexible thin-plate regression spline (Wood 2006). Residuals were assumed to be independent and normally distributed, an assumption that was visually assessed for each model.

To minimize extrapolation beyond the observations, contours of the resulting model standard error were mapped and a threshold was visually chosen by selecting the smallest standard error contour that encompassed all of the observations. For all grid cells within the spatial domain defined by this standard error threshold, egg or larval concentrations within each grid cell were predicted from the GAM fit. The predicted concentrations were then re-scaled to correspond to the fraction of each ELS in each grid cell in each month for comparison with model output. Fractions within each grid cell were used for comparison because the model produces relative concentrations that cannot directly be compared to observed densities.

Model output (longitude, latitude, depth, egg/larval length, time) was treated in the same way as observational data. The output for all seven spawning times was aggregated, since the spawning times of eggs and larvae collected in the field were unknown. The model output was separated by month and pollock ELS. Model output for each stage, month, and year was restricted to those particles that fell within the same spatial domain over which GAM-predicted concentrations were obtained. The fraction of particles within each of the corresponding grid cells was calculated for all stages, months, and years.

The growth and vertical behavior routines were selected using multiple skill metrics (Stow et al. 2009), including correlation coefficient (R), root mean square error (RMSE), and modeling efficiency (MEF), calculated from the GAM-predicted fractions and the modeled fractions for all months with observations in the years 1995 and 2007. All three skill metrics (Table 1) indicated the same two behaviors as the best model: behaviors 1 (passive individuals of all stages) and 2 (passive eggs and yolksac larvae, preflexion and late larvae that move to the middle of the mixed layer). Combined with the two different growth formulas, three of the four combinations were the only simulations that produced results better than using the average of the observations, as denoted by positive modeling efficiencies (Table 1). The resulting depth distributions were not used for model selection, but compare favorably with observations (Figure 4).

2.4.4 Model simulations

Based on the skill results, the warm and cold year simulations were run with temperature-dependent growth and vertical behavior 2 (passive eggs and yolksac larvae, preflexion and late larvae that move to the middle of the mixed layer). After selecting the growth and vertical behavior routines based on results of the 1995 and 2007 simulations, the biophysical model was run for each of the warm (1996, 2002, 2003, 2005) and cold (1997, 1999, 2000, 2006, 2008-2012) years using model output from ROMS NEP6 hindcasts. Years were identified as either warm or cold based on the sign of the sea surface temperature anomaly, following Smart et al. (2012). The modeled egg and larval distributions during warm and cold years were contrasted and related to physical forcing to determine potential mechanisms for the observed differences. A series of simulations was conducted to elucidate if differences in horizontal distributions of pollock ELS between warm and cold years are attributable to spawning timing, spawning location, physical transport, and/or development during transport. All simulations used year-specific physical forcing, but different scenarios for spawning time and location:

(1) Physical transport – The same spawning time and location for both warm and cold years, thus differences in distribution arise from differences in advection alone

(2) Delay spawning time – The same spawning locations, delay initialization of cold year spawning by 40 d

(3) Advance spawning time – The same spawning locations, advance initialization of warm year spawning by 40 d

(4) Contract spawning location – Contract spawning polygons in cold years by shifting the eastern edge of spawning polygons offshore to the southwest (by 0.5° to the South and 0.25° to the West around the Pribilof Islands; by 1.0° to the South and 0.50° to the West around Unimak Island).

(5) Expand spawning location – Expand spawning polygons in warm years by shifting the eastern edge of spawning polygons onshore to the northeast (0.50° to the North, 0.25° to the East).

The advance and delay in spawn timing for scenarios 2 and 3 (40 d) were chosen based on the difference in peak egg abundance between warm and cold years (Smart et al. 2012). The simple contraction and expansion of spawning polygons were used to simulate the exclusion of spawning from areas with sea surface temperatures < 2.4 °C and >3.8 °C based on the statistical model of Barbeaux (2012) that found positive adult pollock winter abundances between these

401 temperatures. The spawning polygons developed for the physical transport run described above
402 were compared to the distribution of ROMS-generated SST for a few warm and cold years.
403 General shifts were created to remove spawning from areas that tended to be <2.4 °C in cold
404 years and to expand spawning in regions usually <3.8 °C. Combinations of scenarios 2 with 4
405 and 3 with 5 were also tested but are not presented, as they did not provide any additional
406 information. Model output of position, velocity, and length was saved at daily increments. Only
407 model output prior to Oct 1 of each year was used to correspond to the observational time period.
408
409 **2.5 Comparisons and statistics**
410 The same 0.25° x 0.25° grid over the eastern Bering Sea was used to constrain the model
411 output of the scenario tests to the spatial regions containing observations in both cold and warm
412 years. Model results were restricted to particles that fell within a grid cell with at least one
413 observation in both a cold and warm year. The fraction of particles within each grid cell
414 containing observations in both cold and warm years was calculated for each stage and each
415 year, from all individuals in a given stage during the whole larval period. The mean fraction of
416 particles in each grid cell was then computed for cold and warm years separately for
417 visualization of the horizontal distributions.
418 To quantify changes in the horizontal distributions, the center of gravity and major and
419 minor axes were calculated for each life stage by employing the approach described in Woillez et
420 al. (2009) and implemented in R (R Development Core Team 2011). The approach calculates the
421 abundance-weighted average latitude and longitude of individuals over a fixed grid of stations.
422 For these calculations we used the midpoint longitude and latitude of each grid cell and the
423 fraction of particles of each life stage occurring in a given grid cell, aggregated over the entire
424 larval period. The overall center of gravity was then computed by thermal regime across 11 cold
425 years and 4 warm years. For comparison, the center of gravity and major and minor axes were
426 similarly calculated for the observations from cold and warm years, also constrained to the same
427 grid cells with observations in both thermal regimes. Correspondingly, longitude and latitude
428 were weighted by the mean concentration of each stage in each grid cell instead of by the
429 fraction of simulated individuals.
430 A second measure of spatial differences, the local index of collocation (LIC), was utilized
431 since multiple distributions can produce the same center of gravity. In contrast to the center of

gravity, the LIC measures local variations in distribution with grid cell-by-grid cell comparisons (Kotwicki & Lauth 2013).

$$LIC = \frac{\sum_{i=1}^{n} z_{i1} z_{i2}}{\sqrt{\sum_{i=1}^{n} z_{i1}^2} \sqrt{\sum_{i=1}^{n} z_{i2}^2}}$$

where z_{i1} and z_{i2} are either the fraction of particles or mean concentration by stage at grid cell i for the two cold and warm simulation distributions being compared. Values of LIC range from 0 to 1, with 0 the most different and 1 the most similar.

3. RESULTS

3.1 Sensitivity of physical transport simulation

In both cold and warm years, there was a noticeable difference only in the late larval centers of gravity in simulations with passive individuals compared to simulations with vertical behavior (Table 2). Including behavior in the model resulted in the center to be more to the east (on-shelf), with a slightly larger difference in warm years. Simulated centers of gravity were more sensitive to the growth formulation than to implementation of vertical behavior. In both cold and warm years, temperature-dependent growth resulted in different centers of gravity for yolksac, preflexion, and late larvae compared to age-dependent growth (Table 2) due to differences in stage duration. The centers of gravity of yolksac and preflexion larvae with temperature-dependent growth were more on-shelf, whereas they were more off-shelf for late larvae. The differences between temperature-dependent and age-dependent centers of gravity were greater in cold years than warm years (Table 2). This stems from the larger difference in growth rates between the age-dependent model and temperature-dependent model at lower temperatures (Figure 2c), resulting in longer stage durations in cold years when growth is temperature-dependent.

The effect of temperature-dependent growth alone on the differences in distribution between warm and cold can be seen by comparing simulations with temperature-dependent growth and either passive or vertical behavior. When passive, eggs and yolksac larvae were more off-shelf while preflexion and late larvae were more on-shelf in warm years (Table 2). The distance between centers of gravity was greater for the yolksac stages than the preflexion and late stages (Table 2). Adding behavior moved the centers of gravity of the egg, yolksac, and late stages eastwards in warm years, resulting in smaller differences between the eggs and yolksac

462 stages, but late larvae shifted even further on-shelf in comparison to cold years (Table 2).
463 Conversely, the center of gravity of preflexion larvae with behavior moved westward in warm
464 years, producing a negligible difference between warm and cold years (Table 2).
465
466 **3.2 Cold vs. warm years**
467 *3.2.1 Observations*
468 Distributions of pollock eggs and larvae from the FOCI survey observations listed in
469 Smart et al. (2012) exhibit large differences in the centers of gravity between cold and warm
470 years ranging from 77 to 186 km (Table 3). Local variations in distribution were also large, with
471 LIC from 0.06 to 0.24 (Table 3). The centers of all the larval stages were more on-shelf to the
472 northeast in warm years, whereas the egg stage showed the reverse pattern (Table 3). The egg
473 stage exhibited the greatest difference in local distribution, whereas the largest difference in
474 centers of gravity occurred in the late larval stage (Table 3).
475
476 *3.2.2 Physical transport*
477 When initial conditions (egg release locations and timing) were held constant across
478 years, such that all differences were due to variation in ocean circulation driven by climate
479 variability, there did not appear to be large differences between the mean horizontal distributions
480 of simulated eggs, yolksac larvae, and late larvae between cold (Figure 5 center) and warm years
481 (Figure 6 center). The distributions of the preflexion larval stage were noticeably different, with
482 individuals more widespread on the outer and middle shelves in cold years (Figure 5 center,
483 Figure 6 center). The differences in the centers of gravity quantify that, on average, the egg,
484 yolksac, and preflexion stages were more westward (off-shelf) in warm years, whereas the late
485 stages were more eastward (Table 3). The distance between the centers of gravity in cold and
486 warm years is small for the egg and preflexion stages, and slightly larger for the yolksac and late
487 larval stages (Table 3).
488
489 *3.2.3 Delay spawning time*
490 Similar to the physical transport scenario, there are no obvious differences between the
491 mean modeled stage distributions between warm and cold years when spawning is delayed 40 d
492 in cold years (Figure 5 left, Figure 6 center). In this case, the distribution of the preflexion larval

493 stage in cold years (Figure 5 left) is more similar to that of preflexion in warm years (Figure 6
494 center). Though the variations in the horizontal distribution from the physical transport case may
495 not be apparent visually, delaying the spawning times resulted in greater differences in the
496 centers of gravity of all stages except the yolksac larvae (Table 3). Preflexion and late larval
497 centers of gravity were more on-shelf in warm years, whereas the eggs and yolksac larvae were
498 slightly more off-shelf (Table 3). The differences between the centers of gravity for warm and
499 cold years were marginal for the egg and yolksac stages, and were largest for the preflexion stage
500 (Table 3). Compared to the physical transport case in cold years, a 40 d delay in spawning
501 changed the distributions of the preflexion and late larvae (Figure 5 left, center). With a delay,
502 the distribution of preflexion larvae was not as widespread as in the physical transport simulation
503 (Figure 5 left, center).
504
505 *3.2.4 Advance spawning time*
506 Spawning 40 d earlier in warm years resulted in fewer preflexion larvae on the outer shelf
507 and more late larvae on the middle shelf (Figure 6 left) in warm years compared to physical
508 transport with normal spawning time in cold years (Figure 5 center). The preflexion distribution
509 was also more widely spread in comparison with physical transport with normal spawning time
510 in warm years (Figure 6 center). Advancing the spawning times resulted in greater differences in
511 the centers of gravity of all life stages compared to the physical transport scenario (Table 3). The
512 yolksac, preflexion, and late stages were more on-shelf in warm years with early spawning, and
513 the centers of gravity grew further apart with stage (Table 3).
514
515 *3.2.5 Contract spawning location*
516 A large difference in the mean horizontal distributions occurred when spawning locations
517 were contracted in cold years. All stages were concentrated on the outer shelf and over the slope
518 in cold year simulations (Figure 5 right), with none over the middle shelf as seen in warm years
519 (Figure 6 center) or physical transport simulations of cold years (Figure 5 center). The centers of
520 gravity of all stages were more eastward in warm years by approximately 1.0-1.5° longitude
521 (Table 3). Spawning contraction in cold years caused the largest changes in the longitudinal
522 center of gravity and total distance between cold and warm years, with the maximum occurring
523 in the preflexion larval stage (Table 3).

524

525 *3.2.6 Expand spawning location*

526 Expansion of the spawning areas onto the shelf in warm years was reflected in the
527 modeled distributions of pollock ELS (Figure 6 right). The preflexion and late larvae were
528 present over the middle shelf to the northeast of the Pribilof Islands, increased in relative
529 concentration over the middle shelf to the northeast of Unimak Island, and decreased in
530 concentration over the slope and outer shelf (Figure 6 right) compared to the transport only case
531 (Figure 5 center). The yolksac stage exhibited the smallest difference in center of gravity
532 between cold and warm years (Table 3). The centers of gravity of all stages were more
533 northeastward in warm years, though the differences between the warm and cold centers of
534 gravity were not as large as when spawning areas were contracted in cold years (Table 3).

535

536 *3.2.7 Comparison with observations*

537 The simulation with spawning locations contracted in cold years produced results with
538 longitudinal and absolute differences most like the observations for the larval stages (Table 3).
539 However, the contracted spawning simulation (Figure 7) and all other simulations (not shown)
540 generated centers of gravity to the northwest of the observed centers of gravity. Additionally, the
541 simulated centers were over the outer shelf or slope, whereas observed centers of gravity of all
542 larval stages in warm years were on the middle shelf (Figure 7). These differences in local
543 distribution patterns were captured with the LIC measures. Most simulations produced LIC
544 values near 1, indicating similar spatial patterns. In contrast, the LIC of observations were much
545 closer to 0, suggesting greater differences in observed spatial patterns between warm and cold
546 years compared to the model results (Table 3).

547

548 4. DISCUSSION

549 Coupled biological-physical modeling simulations revealed the importance of variations
550 in oceanographic conditions between anomalously cold and warm years in the eastern Bering
551 Sea on the transport and distribution of pollock early life stages. Model simulations suggest that
552 the locations of spawning pollock can drive differences in the horizontal distribution of eggs and
553 larvae. It appears that the influence of sea ice on the distribution of spawning pollock via water

554 temperatures impacts the early life stage distributions more than the hydrographic differences
555 between cold and warm years.
556
557 **4.1 Vertical behavior**
558 Variations in egg buoyancy and the vertical behavior of larvae can alter dispersal and are
559 important considerations when developing a biophysical model of fish (Fiksen et al. 2007),
560 which is why five different vertical behavior routines were tested. Ontogenetic changes in egg
561 buoyancy of the Gulf of Alaska pollock population are well understood (Kendall 1994), but egg
562 density differs between the Bering Sea and Gulf of Alaska populations (Kendall 2001), resulting
563 in dissimilar vertical distributions. Over the Bering Sea shelf, eggs tend to be found at depths
564 <100 m with the greatest concentrations in the upper 20 m (Nishiyama et al. 1986, Smart et al.
565 2013). There appear to be changes in buoyancy such that middle stage eggs occur higher in the
566 water column than early and late stage eggs (Nishiyama et al. 1986), which is suggested in
567 laboratory measurements of specific gravity (Kendall 2001), though the spread of laboratory
568 estimates of buoyancy results in a weak pattern that cannot be parameterized with confidence.
569 Egg specific gravity would be expected to affect egg depth in stratified regions, but not in well-
570 mixed areas (Kendall 2001). Eggs were neutrally buoyant in the model formulation that
571 produced distributions that best matched both horizontal and vertical observations of all pollock
572 ELS. Our use of neutrally buoyant eggs in the model is reasonable since pollock eggs are found
573 at all depths in the Bering Sea (Smart et al. 2013), though an empirical relationship between
574 buoyancy and egg age would improve simulations.
575 The model results that corresponded best with observed horizontal and vertical
576 distributions simulated yolksac larvae as neutrally buoyant. The swimming ability of fish larvae
577 increases over time (Olla et al. 1996) and is rather weak until the inflation of a gas bladder by the
578 time of first feeding (Davis & Olla 1992). As yolksac larvae have limited swimming capability
579 and contain a buoyant yolksac, it seems reasonable to model their vertical behavior like eggs, in
580 this case as neutrally buoyant. In addition to best model performance, this assumption is
581 validated by observations of yolksac larvae distributed throughout the upper 100 m on the Bering
582 Sea shelf (Smart et al. 2013). Constraining preflexion and late larvae to the mixed layer with
583 directed swimming towards the middle of the mixed layer performed better in model-observation
584 comparisons than either model formulation with diel vertical migration (DVM). The evidence for

585 DVM of pollock larvae on the Bering Sea shelf is mixed and varies by larval size and location on
586 the inner, middle, or outer shelf (Smart et al. 2013). Though an oversimplification, our vertical
587 behavior for feeding larvae represents active swimming to stay within the depths with high prey
588 abundance.
589 The routine that resulted in the highest model skill simulated eggs and yolksac larvae as
590 neutrally buoyant, and preflexion and late larvae as active swimmers directed towards the center
591 of the mixed layer. This routine only differed from purely passive physical transport for two
592 stages, and as a result the centers of gravity of the stage distributions varied little between
593 models with and without this behavior pattern. Despite multiple vertical behavior routines that
594 tried to represent observed vertical distributions, the second best model did not include any
595 vertical behavior.
596
597 **4.2 Growth**
598 The model results displayed a greater sensitivity to the growth formulation than to
599 vertical behavior. Many of the simulations with age-dependent growth performed better than
600 those with temperature-dependent growth; however, the model formulation with the lowest
601 RMSE and highest modeling efficiency included temperature-based growth. Comparisons of
602 distributions between warm and cold years were made between different ELS, often defined by
603 length. It is possible that temperature effects on growth rates alone could be responsible for
604 differences in distributions. For example, if transport did not differ between warm and cold
605 years, a given stage could be found at a different location in cold years because it took longer to
606 reach that stage, thus it would be further along on its transport trajectory. This was tested by
607 comparing distributions of simulations with neutrally buoyant ELS with temperature-dependent
608 growth. Indeed, there was a difference in the centers of gravity for warm and cold years, with
609 preflexion and late larvae showing the observed pattern of being more on-shelf in warm years.
610 However, the distances between centers of gravity were not as large as those observed or those
611 produced in other simulations (warm expansion, cold contraction), and the addition of behavior
612 removed the pattern in the preflexion stage. However, the difference between warm and cold
613 years increased for late larvae, thus temperature-dependent growth may play an important role in
614 determining where the largest larvae are found.

615 The age-dependent growth rate used in the model simulations was derived from a length-
616 age relationship from larvae collected in the Gulf of Alaska from May through July 1987
617 (Yoklavich & Bailey 1990). This is probably an overestimate for Bering Sea pollock because the
618 Gulf of Alaska experiences warmer temperatures than the Bering Sea (Blood 2002) and these
619 measurements were made at the warmest part of the larval period. Temperatures in the surface
620 layer of the Gulf of Alaska ranged from approximately 7˚C in mid-May to approximately 10˚C
621 in mid-July based on a seasonal model of temperature variability (F. Mueter, unpub. results) fit
622 to data collected at the GAK 1 monitoring station (http://www.ims.uaf.edu/gak1/). The
623 temperature-based growth equations of yolksac and feeding larvae were each parameterized from
624 three data points of fish in a narrow age range (yolksac: 4 dph, feeding: 18-20 dph). These
625 growth rates were measured in laboratory studies of larvae feeding on *Artemia*, which produce
626 lower growth rates compared to a natural assemblage of zooplankton (Porter & Bailey 2007). To
627 account for the nutritional difference between *Artemia* and natural zooplankton, the growth rate
628 equation of feeding larvae was increased. As yolksac larvae still gain some nutrition from their
629 yolksac, this adjustment was not necessary. More data are needed for a better representation of
630 larval pollock growth rates, which are likely to increase with both temperature and larval size
631 (e.g. Hurst et al. 2010).
632 Despite the coarse approximation of temperature-dependent growth, the resulting mean
633 lengths over the larval period compare adequately with field-observed lengths sampled at
634 different times of the year (Siddon et al. 2013). For example, mean model lengths were 15 and
635 18 mm on May 15, 21 and 28 mm on Jun 15, and 34 and 39 mm on Jul 14 for cold and warm
636 years respectively (Figure 8). The observations during cold years 2008-2010 show lengths 4-14
637 mm on May 15, 5-16 mm on Jun 15, and 7-22 mm on Jul 15, followed by a rapid increase to
638 lengths of 35-90 mm after mid-Aug (Figure 8). Modeled growth ceases at 40 mm, thus the
639 longest lengths observed are never attained. The drastic change in observed lengths between May
640 and Aug signifies a shift in energy allocation (Siddon et al. 2013). The modeled size-
641 independent, temperature-dependent growth rate appears to overestimate growth in the earliest
642 larval phases when much of the energy is allocated to morphological development, and
643 underestimate growth in the later larval phases nearing the juvenile transition when growth is
644 primarily somatic (Siddon et al. 2013), suggesting the need for multiple growth rate equations
645 that vary by larval stage. Nevertheless, the model produced juvenile pollock around the same

time as the observed transition. Differences in observed and modeled lengths could be a result of when and where observed fish were spawned compared to modeled individuals. Additionally, there are few observations of fish 20-40 mm because they are large enough to evade traditional plankton nets but too small to be collected with standard trawl gear, implying that the observed size distribution underestimates the true size distribution. This size range is most abundant at a time of year when historically there have been fewer collections, therefore growth during this critical period is poorly understood. Growth in the wild is highly variable and the modeled growth rates of 0.0-0.2 mm d^{-1} are within the 0.12-0.49 mm d^{-1} rates estimated for field-caught Bering Sea pollock larvae (Walline 1985, Jung et al. 2006). If, however, growth is slower in the wild than in the model, the result would be longer stage durations and potentially larger differences in the resulting distributions of later life stages between warm and cold years. This is consistent with the observed differences being larger than the modeled differences (Table 3).

4.3 Interannual climate variability

The modeled centers of distribution of pollock eggs and larvae did not differ much between warm and cold years when spawning time and location were held constant, and when spawning times were delayed by 40 days. These results suggest that climate-related differences in ocean circulation and delays in spawning time were not sufficient to account for the observed changes in pollock early life stage distributions in the eastern Bering Sea. Simulations with the combined impact of interannual variability in ocean currents and in spatial shifts in spawning areas best captured the observed pattern of early life stages located more on-shelf in warm years compared to cold years. In particular, simulations with contraction of the spawning areas off-shelf (to the west and south) created the largest differences between warm and cold centers of gravity.

The modeled differences between warm and cold years in the "physical transport" model are broadly consistent with results from other studies. Mean currents on the middle shelf are relatively weak with current speeds ranging from negligible to about 2 cm s^{-1} near the surface at a mooring site on the middle shelf (Stabeno et al. 2012). However, Stabeno et al. (2012) found marked differences in current speed and direction at M2 between warm and cold years with a difference in east-west velocity on the order of 1-2.5 cm s^{-1}. This implies a difference in expected transport between warm and cold years of approximately 78-195 km over a 90-day period,

677 compared to the estimated difference in the modeled center of gravity for late larvae of 14.6 km
678 (Table 3). A smaller difference in the center of gravity, which reflects the average endpoint, is
679 expected because eggs and larvae generally do not follow straight-line trajectories. Modeled
680 transport is also highly variable over time as evident in the large differences in relative transport
681 between different life stages in our model (Table 3), consistent with seasonal variability in
682 currents (Stabeno et al. 2012).
683 Our analyses focused on differences in transport between warm and cold years, but these
684 differences should not be interpreted as a consequence of temperature variability. Rather,
685 differences in both temperature and transport result from variability in wind forcing, which is
686 associated with variability in along-isobath and cross-isobath advection (Danielson et al 2011b).
687 Cross-isobath fluxes in particular are strongly dependent on wind direction (Danielson et al.
688 2012) as determined by the seasonal mean zonal position of the Aleutian Low (Danielson et al.
689 2011b). Strong winds from the northwest are associated with larger westward transports and cold
690 conditions, while stronger winds from the southeast are associated with enhanced eastward and
691 northward flows and warmer conditions (Danielson et al. 2011b, 2012). However, winds during
692 warm (cold) years are not always favorable to on-shelf (off-shelf) Ekman transport; therefore the
693 differences in modeled transport between warm and cold years in this study may underestimate
694 the importance of physical transport.
695 Nevertheless, model results suggest that spatial shifts in spawning distribution underlie
696 the shifts in egg and larval distributions. There is a significant lack of empirical information on
697 the factors regulating where and when adults spawn. We propose that sea ice and water
698 temperature affect the pollock spawning distribution in the eastern Bering Sea. Some support for
699 our hypothesis comes from 30 years of summer (May-Aug) bottom trawl survey data that
700 demonstrates an effect of the areal extent of the cold pool defined at 0 °C on the eastern Bering
701 Sea pollock distribution (Kotwicki & Lauth 2013). Adult distributions were compared in a
702 pairwise manner, such that the distribution from each year was compared individually to the
703 distributions from the 29 other years. The similarity between distributions from all years
704 decreased with increases in the change of the cold pool extent (Kotwicki & Lauth 2013).
705 Resembling the larval distributions, the center of gravity of adult summer distributions differed
706 between warm and cold years, with centers located 42 km off-shelf in cold years (Kotwicki &
707 Lauth 2013).

Thermally influenced shifts in adult distributions, spawning migrations, and ELS distributions have been noted for a number of species, such as Atlantic Cod (*Gadus morhua*; deYoung & Rose 1993) and Capelin (*Mallotus villosus*; Rose 2005), in addition to Bering Sea (Bacheler et al. 2012) and Gulf of Alaska (Bacheler et al. 2009) pollock stocks. Although Bacheler et al. (2012) found low interannual variability in the spatial and temporal dynamics of Bering Sea pollock spawning, there were changes in the abundance of adults and eggs with temperature. With 1 °C of warming a spatially explicit variable coefficient generalized additive model predicted increased egg abundance over the middle shelf to the east of the Pribilof Islands and increased adult CPUE over the middle shelf north of Unimak Island (Bacheler et al. 2012). Though the broad spawning area may not have shifted, the changes in spawner and egg abundance on the middle shelf shift the distribution within this region, resulting in greater egg production on-shelf with warmer conditions. Similarly, Bacheler et al. (2009) found spatial effects of spawning stock biomass, transport, and temperature on pollock egg abundance in Shelikof Strait. With increased temperature, egg abundance increased around the northern edge of Kodiak Island and decreased in the southwest of Shelikof Strait (Bacheler et al. 2009), suggesting shifts in spawning areas with temperature. A review of data on Newfoundland Atlantic Cod by deYoung and Rose (1993) provided evidence for shifts in adult and larval distributions in relation to temperature with a link to recruitment. They found more southerly distributions of adults in cold years that resulted in more southerly distributions of eggs and larvae, placing them in regions with lower retention (deYoung & Rose 1993). They posited that the reduced recruitment in cold years was a consequence of larvae spending less time on the shelf (deYoung & Rose 1993).

Much like the temperature-induced changes in spawning and larval distributions of Atlantic Cod off Newfoundland, the eastern Bering Sea pollock ELS distributions varied with respect to local circulation. The differences in centers of gravity between the simulations of warm years with regular spawning and cold years with off-shelf contracted spawning (Table 3, "Contracted") arise from the lack of eggs and larvae on the middle shelf off Unimak Island and the Alaskan Peninsula in cold years (Figure 3). This difference highlights the importance of the spatial variability of the currents on the eastern Bering Sea shelf. Contraction of spawning off-shelf reduces the number of eggs and larvae exposed to the cross-shelf currents near Unimak Island, including the Alaska Coastal Current, while increasing the proportion of eggs and larvae

739 exposed to more energetic along-shelf currents over the outer shelf and slope (Figure 1). There is
740 also retentive circulation around the Pribilof Islands (Kowalik & Stabeno 1999; Figure 1) that
741 may have facilitated the presence of pollock on the middle shelf when spawning was shoalward
742 of the 100-m isobath in the simulations without contracted spawning.
743 The model results emphasize the interdependencies of cross-shelf transport and thermal
744 regime to pollock ELS and of spawning near cross-shelf features. Tests of spawning distributions
745 were implemented as generalized off-shelf or on-shelf contractions or expansions because a
746 consistent observational data set of adults in spawning condition that spanned cold and warm
747 years was not available. The hypothetical variations in spawning areas were constructed from a
748 relationship between SST and adult pollock winter abundance (Barbeaux 2012), though these
749 shifts were imprecise. More realistic spawning locations could be generated for each year using
750 the annual distributions of SST and initializing eggs in places with SST between 2.4 and 3.8 °C.
751 A better approach would be to formulate a relationship between water temperature and the
752 presence of adult pollock in spawning condition.
753
754 **4.4 Expectations with climate change**
755 Projections with Intergovernmental Panel on Climate Change climate models predict
756 decreased sea ice extent and increased sea surface temperatures in the eastern Bering Sea (Wang
757 et al. 2012), conditions much like the warm years of 2002-2005. During these warm years the
758 abundance of large, energy-rich zooplankton decreased and abundance of small, energy-poor
759 zooplankton increased (Coyle et al. 2011). The asymmetric effect of temperature on zooplankton
760 development and growth suggest that the typically large, energy-rich copepods would have been
761 smaller with fewer lipid reserves in warm years as well (Coyle et al. 2011). The shift in the
762 zooplankton community has a two-fold effect on young pollock. Firstly, the decrease in lipid-
763 rich prey would decrease the energy density of age-0 pollock, thereby reducing the probability of
764 overwinter survival (Moss et al. 2009, Heintz et al. 2013). Secondly, age-0 pollock experience
765 increased predation pressure from predatory fishes that would otherwise feed on the large,
766 energy-rich zooplankton (Moss et al. 2009, Coyle et al. 2011). Combined, the decreased energy
767 reserves for overwintering and increased predation pressure suggest lower pollock survival and
768 recruitment in warm years.

769 Changes in ice extent and water temperatures are expected to alter the distribution of
770 spawning pollock adults. Model simulations demonstrated that simplified expansions and
771 contractions of the spawning areas affect the distributions of pollock ELS. Going beyond
772 distributions, it is important to understand how transport pathways and connectivity differ
773 between warm and cold years. Future studies will examine how potential prey and predators
774 overlap spatially and temporally with ELS of pollock during transport and with the end (summer)
775 distribution of juveniles (age-0s) in warm and cold years. To this end, we will investigate if
776 variations in the transport pathways between warm and cold years contribute to recruitment
777 variability, or if recruitment is more strongly related to annual shifts in the zooplankton
778 community and processes that occur during the transition from age-0 to age-1.
779
780 **4.5 Considerations**
781 The model simulations with contracted spawning areas in cold years qualitatively
782 captured the observed difference in horizontal distributions of pollock larvae between cold and
783 warm years, although the modeled and observed distributions of ELS differed. The observed
784 centers of gravity of all larval stages were more on-shelf in warm years, but both cold and warm
785 centers were located further southeast than the simulation results. Moreover, the observed centers
786 of gravity in warm years were over the middle shelf, whereas the modeled centers were over the
787 outer shelf in all warm year simulations. In contrast to Smart et al. (2012), who inferred no
788 temperature effect on egg distribution, we found that egg centers of gravity were more off-shelf
789 in warm years.
790 There are a number of potential reasons that the model did not completely replicate the
791 observed distributions of pollock eggs and larvae. One explanation is related to the differences
792 between the observations and model results. The observations were collected in the months of
793 March through September, while the model represented the months January through September.
794 As indicated by the Smart et al. (2012) analysis, the field sampling missed the start and peak of
795 the egg stage and the start of the yolksac stage in warm years, and the end of the late larval stage
796 in cold years. Thus the observations may not represent the true distribution of these life stages in
797 these years. Additionally, the monthly observations and model results were aggregated by year,
798 and then by cold or warm period, rather than compared at particular times and locations.
799 Observations occurred at discrete locations, whereas modeled particles essentially covered the

800 eastern Bering Sea. Though the model results were restricted to only particles in areas that were
801 sampled in both warm and cold years, this could contribute to divergences. Second, actual
802 spawning times and locations may result in simulated distributions more similar to the
803 observations than the generalized spawning used in this research, as mentioned above. Third,
804 spatial and temporal variability in both egg production and the mortality of all stages, and their
805 seasonal and interannual changes, could significantly shape the distribution of pollock eggs and
806 larvae. The difference in LIC measures between observations and simulations (Table 3) provide
807 strong support for spatially-variable processes. As this study was focused on interannual
808 differences in advection, these spatial variations were not considered because they could have
809 masked the effect of physical transport alone.
810
811 5. CONCLUSIONS
812 We developed a biophysical model that was able to replicate important features of the
813 observed distributions of eggs and larvae of Walleye Pollock in the eastern Bering Sea. An
814 advantage of this modeling approach was the ability to individually test environmental forcing
815 mechanisms to quantitatively assess the impact of each on the distribution of pollock. Interannual
816 variations in advection and advances and delays in spawning time were insufficient at
817 reproducing the observed differences in pollock early life stage distributions between warm and
818 cold years in the eastern Bering Sea. Changes to spawning areas, especially offshore contractions
819 in cold years, resulted in simulated distributions most similar to observations. The location of
820 spawning with respect to cross-shelf circulation patterns was an important factor influencing the
821 distribution of eggs and larvae. Further study is needed on the relationship between the spatial
822 distribution of spawning pollock and the physical environment, and its effect on the distribution
823 of early life stages. Based on our model results, future investigations will include how warm and
824 cold year variations in distribution correlate with recruitment and how they affect age-0 survival
825 by way of spatial overlaps with potential prey and predators.
826
827 ACKNOWLEDGEMENTS
828 This manuscript benefitted from data provided by and discussions with Steve Barbeaux,
829 Seth Danielson, and Elizabeth Siddon, the research completed by the BEST-BSIERP program,
830 and reviews by Sarah Hinckley, Ann Matarese, Jeff Napp, Myron Peck, and two anonymous

reviewers. We thank Frederic Castruccio for his initial work with ROMS and TRACMASS. This research was funded by NSF award 1108440. This research is EcoFOCI-0811 to NOAA's Fisheries-Oceanography Coordinated Investigations and BEST-BSIERP contribution number ###. The findings and conclusions in the paper are those of the authors and do not necessarily represent the views of the National Marine Fisheries Service.

REFERENCES

Bacheler, N.M, Bailey, K.M., Cianelli, L., Bartolino, V., Chan, K.-S. 2009. Density-dependent, landscape, and climate effects on spawning distribution of walleye pollock *Theragra chalcogramma*. Marine Ecology Progress Series 391, 1-12.

Bacheler, N.M., Ciannelli, L., Bailey, K., Duffy-Anderson, J.T. 2010. Spatial and temporal patterns of walleye pollock (*Theragra chalcogramma*) spawning in the eastern Bering Sea inferred from egg and larval distributions. Fisheries Oceanography 19, 107-120.

Barbeaux, S.J. 2012. Scientific acoustic data from commercial fishing vessels: eastern Bering Sea walleye pollock (*Theragra chalcogramma*). Ph.D. Thesis, University of Washington.

Blanke, B., Raynaud, S. 1997. Kinematics of the Pacific Equatorial Undercurrent: a Eulerian and Lagrangian approach from GCM results. Journal of Physical Oceanography 27, 1038-1053.

Blood, D.M. 2002. Low-temperature incubation of walleye pollock (*Theragra chalcogramma*) eggs from the southeast Bering Sea shelf and Shelikof Strait, Gulf of Alaska. Deep-Sea Research II 49, 6095-6108.

Brickman, D., Adlandsvik, B., Thygesen, U.H., Parada, C., Rose, K., Hermann, A.J., Edwards, K. 2009. Particle tracking. In: Manual of recommended practices for modeling physical-biological interactions during fish early life. Eds. North, E.W., Gallego, A., Petitgas, P. ICES Cooperative Research Report No. 295, pp 9-19.

862 Budgell, W. 2005. Numerical simulation of ice-ocean variability in the Barents Sea region.
863 Ocean Dynamics 55, 370–387.
864
865 Canino, M.F. 1994. Effects of temperature and food availability on growth and RNA/DNA ratios
866 of walleye pollock *Theragra chalcogramma* (Pallas) eggs and larvae. Journal of Experimental
867 Marine Biology and Ecology 175, 1-16.
868
869 Carton, J.A., Giese, B.S. 2008. A reanalysis of ocean climate using Simple Ocean Data
870 Assimilation (SODA). Monthly Weather Review 136, 2999-3017.
871
872 Coachman, L.K. 1986. Circulation, water masses, and fluxes on the southeastern Bering Sea
873 shelf. Continental Shelf Research 5, 23-108.
874
875 Coyle, K.O., Eisner, L.B., Mueter, F.J., Pinchuk, A.I., Janout, M.A., Cieciel, K.D., Farley, E.V.,
876 Andrews, A.G. 2011. Climate change in the southeastern Bering Sea: impacts on pollock stocks
877 and implications for the oscillating control hypothesis. Fisheries Oceanography 20, 139-156.
878
879 Curchitser, E.N., Haidvogel, D.B., Hermann, A.J., Dobbins, E.L., Powell, T.M., Kaplan, A.
880 2005. Multi-scale modeling of the North Pacific Ocean: Assessment and analysis of simulated
881 basin-scale variability (1996–2003). Journal of Geophysical Research 110, C11021,
882 doi:10.1029/2005JC002902.
883
884 Curchitser, E.N., Hedstrom, K., Danielson, S., Weingartner, T.J. 2010. Modeling the circulation
885 in the North Aleutian Basin. Department of Interior, OCS Study BOEMRE 2010-028.
886
887 Dai, A., Trenberth, K.E. 2002. Estimates of freshwater discharge from continents: Latitudinal
888 and seasonal variations. Journal of Hydrometeorology 3, 660-687. doi:10.1175/1525–
889 7541(2002)003<0660:eofdfc>2.0.co;2
890

Danielson, S., Curchitser, E., Hedstrom, K., Weingartner, T., Stabeno, P. 2011a. On ocean and sea ice modes of variability in the Bering Sea. Journal of Geophysical Research 116, C12034, doi:10.1029/2011JC007389

Danielson, S., Eisner, L., Weingartner, T., Aagaard, K. 2011b. Thermal and haline variability over the central Bering Sea shelf: seasonal and interannual perspectives. Continental Shelf Research 31, 539-554.

Danielson, S., Hedstrom, K., Aagaard, K., Weingartner, T., Curchitser, E., 2012. Wind-induced reorganization of the Bering shelf circulation. Geophysical Research Letters 39, L08601-L08606.

Davis, M.W., Olla, B.L. 1992. Comparison of growth, behavior and lipid concentrations of walleye pollock *Theragra chalcogramma* larvae fed lipid-enriched, lipid-deficient and field-collected prey. Marine Ecology Progress Series 90, 23-30.

de Vries, P., Döös, K. 2001. Calculating Lagrangian trajectories using time-dependent velocity fields. Journal of Atmospheric and Oceanic Technology 18, 1092-1101.

deYoung, B., Rose, G.A. 1993. On recruitment and distribution of Atlantic cod (*Gadus morhua*) off Newfoundland. Canadian Journal of Fisheries and Aquatic Sciences 50, 2729-2741.

Döös, K. 1995. Inter-ocean exchange of water masses. Journal of Geophysical Research 100, 13499-13514.

Döös, K., Engqvist, A. 2007. Assessment of water exchange between a discharge region and the open sea: a comparison of different methodological concepts. Estuarine, Coastal and Shelf Science 74, 585-597.

Drijfhout, S., de Vries, P., Döös, K., Coward, A. 2003. Impact of eddy-induced transport of the Lagrangian structure of the upper branch of the thermohaline circulation. Journal of Physical Oceanography 33, 2141-2155.

Duffy-Anderson, J., Smart, T.I., Siddon, E.C., Heintz, R., Farley, E., Horne, J., Parker-Stetter, S., Ressler, P., Barbeaux, S., Petrik, C.M. *In review*. A synthesis of the ecology of walleye pollock (*Theragra chalcogramma*) in the eastern Bering Sea during the first year of life. Deep-Sea Research II.

Dunn, J.R., Matarese, A.C. 1987. A review of the early life history of northeast Pacific gadoid fishes. Fisheries Research 5, 163-184.

Engqvist, A., Döös, K., Andrejev, O. 2006. Modeling water exchange and contaminant transport through a Baltic Coastal region. Ambio 35, 435-447.

Fiksen, Ø., Jørgensen, C., Kristiansen, T., Vikebø, F., Huse, G. 2007. Linking behavioural ecology and oceanography: larval behavior determines growth, mortality, and dispersal. Marine Ecology Progress Series 347, 195-205.

Heintz, R.A., Siddon. E.C., Farley, Jr., E.V., Napp, J.M. 2013. Correlation between recruitment and fall condition of age-0 walleye pollock (*Theragra chalcogramma*) from the eastern Bering Sea under varying climate conditions. Deep-Sea Research II 94, 150-156.

Hermann, A.J., Curchitser, E.N., Dobbins, E.L., Haidvogel, D.B. 2009. A comparison of remote versus local influence of El Niño on the coastal circulation of the Northeast Pacific. Deep-Sea Research II 56, 2427-2443. doi:10.1016/j.dsr2.2009.02.005.

Hinckley, S. 1987. The reproductive biology of walleye pollock, *Theragra chalcogramma*, in the Bering Sea, with reference to spawning stock structure. Fisheries Bulletin U.S. 85, 481-498.

950 Hunke, E., Dukowicz, J. 1997. An elastic-viscous-plastic model for sea ice dynamics. Journal of
951 Physical Oceanography 27, 1849-1867.
952
953 Hurst, T.P., Laurel, B.J., Ciannelli, L. 2010. Ontogenetic patterns and temperature-dependent
954 growth rates in early life stage of Pacific cod (*Gadus macrocephalus*). Fisheries Bulletin108,
955 382-392.
956
957 HYCOM Ocean Prediction website. http://hycom.org/ocean-prediction. Last accessed 25 Nov
958 2013.
959
960 Ianelli, J.N., Barbeaux, S.J., McKelvey, D., Honkalehto, T. 2012a. Assessment of walleye
961 pollock in the Bogoslof Island Region. In: Stock assessment and fishery evaluation report for the
962 groundfish resources of the Bering Sea/Aleutian Islands regions. North Pacific Fishery
963 Management Council, 605 W. 4th Ave., Suite 306, Anchorage, AK. pp. 235-244
964
965 Ianelli, J.N., Honkalehto, T., Barbeaux, S., Kotwicki, S., Aydin, K., Williamson, N. 2012b.
966 Assessment of the Walleye Pollock stock in the Eastern Bering Sea. *In* Stock assessment and
967 fishery evaluation report for the groundfish resources of the Bering Sea/Aleutian Islands regions.
968 North Pacific Fishery Management Council, 605 W. 4th Ave., Suite 306, Anchorage, AK 99501.
969 pp. 51-156.
970
971 Jung, K.-M., Kang, S., Kim, S., Kendall, Jr., A.W. 2006. Ecological characteristics of walleye
972 pollock eggs and larvae in the southeastern Bering Sea during the late 1970s. Journal of
973 Oceanography 62, 859-871.
974
975 Kendall, Jr., A.W. 1994. The vertical distribution of eggs and larvae of walleye pollock,
976 *Theragra chalcogramma*, in Shelikof Strait, Gulf of Alaska. Fisheries Bulletin 92, 540-554.
977
978 Kendall, Jr., A.W. 2001. Specific gravity and vertical distribution of walleye pollock (*Theragra*
979 *chalcogramma*) eggs. NOASA/AFSC Processed Report 2001-01. 92p.
980

Kotwicki, S., Lauth, R.R. 2013. Detecting temporal trends and environmentally-driven changes in the spatial distribution of bottom fishes and crabs on the eastern Bering Sea shelf. Deep-Sea Research II 94, 231-243.

Kowalik, Z., Stabeno, P.J. 1999. Trapped motion around the Pribilof Islands in the Bering Sea. J. Geophys. Res. 104, 25667-25684.

Lanksbury, J.A., Duffy-Anderson, J.T., Mier, K.L., Busby, M.S., Stabeno, P.J. 2007. Distribution and transport patterns of northern rock sole, *Lepidopsetta polyxystra*, larvae in the southeastern Bering Sea. Progress in Oceanography 72, 39-62.

Large, W.G., McWilliams, J.C., Doney, S.C. 1994. Oceanic vertical mixing: a review and a model with a nonlocal boundary layer parameterization. Review of Geophysics 29, 363-403.

Large, W.G., Yeager, S.G. 2009. The global climatology of an interannually varying air-sea flux data set. Climate Dynamics 33, 341-364. doi:10.1007/s00382-008-0441-3.

Matarese, A.C., Kendall, Jr., A.W., Blood, D.M., Vinter, B.M. 1989. Laboratory guide to early life history stages of northeast Pacific fishes. NOAA/National Marine Fisheries Service, NOAA Technical Report NMFS 80. 652p.

Mellor, G.L., Kantha L. 1989. An ice-ocean coupled model. Journal of Geophysical Research 94, 10937-10954.

Mizobata, K., Saitoh, S., Wang, J. 2008. Interannual variability of summer biochemical enhancement in relation to Mesoscale eddies at the shelf break in the vicinity of the Pribilof Islands, Bering Sea. Deep-Sea Research II 55, 1717-1728.

Moss, J.H., Farley, Jr., E.V., Feldman, A.M., Ianelli, J.N. 2009. Spatial distribution, energetic status, and food habits of eastern Bering Sea age-0 walleye pollock. Transactions of the American Fisheries Society 138, 497-505.

Mueter, F.J., Litzow, M.A. 2008. Sea ice retreat alters the biogeography of the Bering Sea continental shelf. Ecological Applications 18, 309-320.

Nishiyama, T., Hirano, K., Haryu, T. 1986. The early life history and feeding habits of larval walleye pollock, *Theragra chalcogramma* (Pallas), in the southeast Bering Sea. INPFC Groundfish Symposium Paper No. P-10.

Olla, B.I, Davis, M.W., Ryer, C.H., Sogard, S.M. 1996. Behavioural determinants of distribution and survival in early stages of walleye pollock, *Theragra chalcogramma*, a synthesis of experimental studies. Fisheries Oceanography 5, 167-171.

Peck, M.A., Buckley, L.J., Bengtson, D.A. 2006. Effects of temperature and body size on the swimming speed of larval and juvenile Atlantic cod (*Gadus morhua*): implications for individual-based modeling. Environmental Biology of Fishes 75, 419-429. doi 10.1007/s10641-006-0031-3.

Porter, S.M., Bailey, K.M. 2007. Optimization of feeding and growth conditions for walleye pollock *Theragra chalcogramma* (Pallas) larvae reared in the laboratory. AFSC Processed Report 2007-06. Alaska Fisheries Science Center, NOAA, National Marine Fisheries Service, 7600 Sand Point Way NE, Seattle WA 98115. 20p.

R Development Core Team. 2011. R: A language and environment for statistical computing. R Foundation for Statistical Computing, Vienna, Australia.

Rienecker, M.M., Suarez, M.J., Gelaro, R., Todling, R., Bacmeiseter, J., Liu, E., Bosilovich, M.G., Schubert, S.D., Takacs, L., Kim, G.-K., Bloom, S., Chen, J., Collins, D., Conaty, A., da Silva, A., Gu, W., Joiner, J., Koster, R.D., Lucchesi, R., Molod, A., Owens, T., Pawson, S., Pegion, P., Redder, C., Reichle, R., Robertson, F.R., Ruddick, A.G., Sienkiewicz, M., Woolen, J. 2011. MERRA: NASA's modern-era retrospective analysis for research and applications. Journal of Climate 24, 3624-3648. doi:10.1175/jcli-d-11–00015.1

Rose, G.A. 2005. Capelin (*Mallotus villosus*) distribution and climate: a sea "canary" for marine ecosystem change. ICES Journal of Marine Science 62, 1524-1530.

Shchepetkin, A.F., McWilliams, J.C. 2009. Ocean forecasting in terrain-following coordinates: Formulation and skill assessment of the regional ocean modeling system. Journal of Computational Physics 228, 8985-9000. doi :10.1016/j.jcp.2009.09.002.

Siddon, E.C., Heinz, R.A., Mueter, F.J. 2013. Conceptual model of energy allocation in walleye pollock (*Theragra chalcogramma*) from age-0 to age-1 in the southeastern Bering Sea. Deep-Sea Research II 94, 140-149.

Smart, T.I., Duffy-Anderson, J.T, Horne, J.K. 2012. Alternating temperature states influence walleye pollock early life stages in the southeastern Bering Sea. Marine Ecology Progress Series 455, 257-267.

Smart, T.I., Siddon, E.C., Duffy-Anderson, J.T. 2013. Vertical distributions of the early life stages of walleye pollock (*Theragra chalcogramma*) in the Southeastern Bering Sea. Deep-Sea Research II 94, 201-210.

Stabeno, P. J., Bond, N. A., Kachel, K. B., Salo, S. A., Schumacher, J. D., 2001. Temporal variability in the physical environment over the southeastern Bering Sea. Fisheries Oceanography 10, 81-98.

Stabeno, P.J., Kachel, N., Mordy, C., Righi, D., Salo, S. 2008. An examination of the physical variability around the Pribilof Islands in 2004. Deep-Sea Research II 55, 1701-1716.

Stabeno, P.J., Kachel, N.B., Moore, S.E., Napp, J.M., Sigler, M., Yamaguchi, A., Zerbini, A.N. 2012. Comparison of warm and cold years on the southeastern Bering Sea shelf and some implications for the ecosystem. Deep-Sea Research II 65-70, 31-45.

1074 Steele, M., Morison, J., Ernold, W., Rigor, I., Ortmeyer, M., Shimada, K. 2004. The circulation
1075 of summer Pacific haloclines water in the Arctic Ocean. Journal of Geophysical Research 109,
1076 C02027, 10.1029/2003JC002009.
1077
1078 Stow, C.A., Joliff, J., McGillicuddy, D.J., Doney, S.C., Allen, J.I., Friedrichs, M.A.M., Rose, K.,
1079 Wallhead, P. 2009. Skill assessment for coupled biological/physical models of marine systems.
1080 Journal of Marine Systems 76, 4-15.
1081
1082 Walline, P.D. 1985. Growth of larval walleye pollock related to domains within the SE Bering
1083 Sea. Marine Ecology Progress Series 21, 197-203.
1084
1085 Wang, M., Overland, J.E., Stabeno, P.J. 2012. Future climate models of the Bering and Chukchi
1086 Seas projected by global climate models. Deep-Sea Research II 65-70, 46-57.
1087
1088 Wespestad, V.G., Fritz, L.W., Ingraham, W.J., Megrey, B.A. 2000. On relationships between
1089 cannibalism, climate variability, physical transport, and recruitment success of Bering Sea
1090 walleye pollock (*Theragra chalcogramma*). ICES Journal of Marine Science 57, 272-278.
1091
1092 Wilderbuer, T., Stockhausen, W., Bond, N. 2013. Updated analysis of flatfish recruitment
1093 response to climate variability and ocean conditions in the Eastern Bering Sea. Deep-Sea
1094 Research II 94, 157-164.
1095
1096 Woillez, M., Rivoirard, J., Petitgas, P. 2009. Notes on survey-based spatial indicators for
1097 monitoring fish populations. Aquatic Living Resources 22, 155-164.
1098
1099 Wood, S.N. 2006. Generalized additive models: an introduction with R. Chapman and Hall/CRC
1100 Press, Boca Raton, FL. 410p.
1101
1102 Yoklavich, M.M., Bailey, K.M. 1990. Hatching period, growth and survival of young walleye
1103 pollock *Theragra chalcogramma* as determined from otolith analysis. Marine Ecology Progress
1104 Series 64, 13-23.

TABLES

Table 1. Resulting skill metrics of the combined comparisons between 1995 and 2007 observations with model results using the different vertical behavior and growth parameterizations. 1 – passive = passive (neutrally buoyant) individuals of all stages; 2 – pre & late MLD = passive eggs and yolksac larvae, and preflexion and late larvae that move to the middle of the mixed layer; 3 – all MLD = all stages move to the middle of the mixed layer; 4 – late DVM = eggs, yolksac, and preflexion larvae move to the middle of the mixed layer, and late larvae make diel vertical migrations (DVMs) between 20 m during the day and 5 m during the night; 5 – pre & late DVM = eggs and yolksac larvae move to the middle of the mixed layer, and preflexion and late larvae make DVMs; age = age-dependent growth; temperature = temperature-dependent growth; R = correlation coefficient; RMSE = root mean square error; MEF = modeling efficiency.

		Skill metric		
Behavior	Growth	R	RMSE	MEF
1 - passive	age	0.12	0.0036	0.03
	temperature	0.11	0.0040	-0.19
2 - pre & late MLD	age	0.10	0.0036	0.03
	temperature	0.11	0.0035	0.10
3 - all MLD	age	0.07	0.0040	-0.18
	temperature	0.06	0.0044	-0.43
4 - late DVM	age	0.07	0.0040	-0.17
	temperature	0.06	0.0044	-0.43
5 - pre & late DVM	age	0.08	0.0040	-0.18
	temperature	0.04	0.0060	-1.66

Table 2. Center of gravity (COG) sensitivity to behavior and growth. Values for longitude and latitude are differences in the COG (°E and °N, respectively) between scenarios: Behavior minus Passive, Temperature minus Age, or Warm minus Cold (where Behavior = vertical behavior of feeding stages; Passive = all stages neutrally buoyant; Temperature = temperature-dependent growth; Age = age-based length (temperature-independent growth); Warm = warm years combined; Cold = cold years combined). Values for Distance are the corresponding absolute distances (km) between COGs.

			Stage			
			Egg	Yolksac	Preflexion	Late
Behavior - Passive	Longitude	Cold	-0.01	-0.01	0.03	0.09
		Warm	0.00	-0.02	0.04	0.15
	Latitude	Cold	0.00	0.00	0.01	0.11
		Warm	0.00	0.00	0.02	0.15
	Distance	Cold	0.54	0.47	2.31	13.32
		Warm	0.01	0.97	3.00	19.56
Temperature - Age	Longitude	Cold	0.00	1.33	0.35	-0.77
		Warm	0.00	0.31	0.44	-0.43
	Latitude	Cold	0.00	-0.04	-0.02	-0.03
		Warm	0.00	0.00	-0.01	-0.01
	Distance	Cold	0.00	83.20	22.22	48.31
		Warm	0.00	19.15	27.55	26.67
Warm - Cold (Temperature)	Longitude	Passive	-0.05	-0.76	0.37	0.34
		Behavior	-0.04	-0.23	-0.02	0.84
	Latitude	Passive	0.00	0.00	0.00	0.07
		Behavior	0.00	-0.01	-0.01	0.04
	Distance	Passive	2.85	47.59	22.82	22.66
		Behavior	2.32	14.54	1.59	52.60

Table 3. Center of gravity (COG) differences and Local Index of Colocation (LIC) between warm and cold years for observations and different simulations. Values for ΔCOG longitude and latitude are differences (°E and °N, respectively) as warm minus cold. Values for Distance are the corresponding absolute distances (km) between COGs. Observed = observations from the cruises listed in Smart et al. 2012; Transport = physical transport; Delay = 40 d delay in cold years; Early = 40 d early in warm years; Contract = contract off-shelf in cold years; Expand = expand on-shelf in warm years.

		Stage			
		Egg	Yolksac	Preflexion	Late
ΔCOG Longitude	Observed	-1.71	1.26	1.14	2.92
	Transport	-0.04	-0.23	-0.09	0.11
	Delay	-0.04	-0.01	0.63	0.24
	Early	-0.05	0.09	0.43	0.79
	Contract	0.96	1.24	1.62	1.24
	Expand	0.29	0.18	0.32	0.49
ΔCOG Latitude	Observed	-0.41	0.19	0.25	0.28
	Transport	0.00	-0.01	-0.02	0.12
	Delay	0.02	0.01	0.01	0.15
	Early	0.02	-0.01	0.08	0.19
	Contract	-0.01	-0.08	-0.13	0.05
	Expand	0.08	0.08	0.09	0.14
COG Distance (km)	Observed	116.98	82.00	76.69	185.85
	Transport	2.31	14.37	6.11	14.63
	Delay	3.32	1.55	39.19	22.65
	Early	4.05	5.88	28.20	53.60
	Contract	59.69	77.74	101.33	76.98
	Expand	20.18	14.41	22.74	34.29
LIC	Observed	0.061	0.240	0.222	0.088
	Transport	0.998	0.983	0.940	0.941
	Delay	0.996	0.986	0.925	0.931
	Early	0.998	0.971	0.920	0.898
	Contract	0.953	0.935	0.815	0.840
	Expand	0.986	0.982	0.937	0.925

1152 FIGURE CAPTIONS

1153 **Figure 1.** The dominant currents (blue lines) and Walleye Pollock spawning areas (green ovals)
1154 of the Eastern Bering Sea. The Alaska coastline is shown in black and the 50, 100, and 200 m
1155 isobaths in gray. ACC – Alaska Coastal Current; BSC – Bering Slope Current.
1156
1157 **Figure 2.** (a) Temperature-dependent egg development time. (b) Temperature-dependent growth
1158 rates of yolksac and feeding (preflexion and late) larvae; growth rate is independent of size. (c)
1159 Length of larvae with age-dependent ("age", solid line) and temperature-dependent (dotted and
1160 dashed lines) growth rates given constant temperature.
1161
1162 **Figure 3.** Spawning initial locations released on the dates shown. Light grey = Cold Contracted;
1163 Dark grey = Transport; Black = Warm Expanded. Polygons are overlapping and all share the
1164 same western and southern boundaries.
1165
1166 **Figure 4.** Depth distribution of early life stages from observations (black) compared to the
1167 model parameterization with the highest skill in reproducing horizontal distributions (grey). This
1168 model had temperature-based growth and vertical behavior 2 – passive eggs and yolksac larvae,
1169 and preflexion and late larvae that move to the middle of the mixed layer. Depth distribution is
1170 presented as a histogram of the weighted mean depth of each MOCNESS tow (observations) or
1171 each day (model).
1172
1173 **Figure 5**. Contour plots of the relative concentration of early life stages in cold year (1995, 1997,
1174 1999, 2000, 2006-2012) simulations. Relative concentration was calculated as the fraction of the
1175 mean number of particles found in each grid cell with observations. 40 d Late = spawning times
1176 delayed by 40 d; Transport Only = same times and locations of spawning in cold and warm
1177 years; Contracted = spawning locations contracted to the southwest.
1178
1179 **Figure 6.** Contour plots of the relative concentration of early life stages in warm year (1996,
1180 2002, 2003, 2005) simulations. Relative concentration was calculated as the fraction of the mean
1181 number of particles found in each grid cell with observations. 40 d Early = spawning times

advanced by 40 d; Transport Only = same times and locations of spawning in cold and warm years; Expanded = spawning locations expanded to the northeast.

Figure 7. Observed (circles) and simulated Contracted (triangles) centers of gravity, major axes, and minor axes for the distributions of different pollock early life stages in cold (blue; 1995, 1997, 1999, 2000, 2006-2012) and warm (red; 1996, 2002, 2003, 2005) years.

Figure 8. Mean standard length (mm) of all larvae by date in the Transport Only simulations for cold (black line; 1995, 1997, 1999, 2000, 2006-2012) and warm (grey line; 1996, 2002, 2003, 2005) years. Standard length (mm) of larval and juvenile pollock from observations in 2008-2010 (dots).

Figure 1. The dominant currents (blue lines) and walleye pollock spawning areas (green ovals) of the Eastern Bering Sea. The Alaska coastline is shown in black and the 50, 100, and 200 m isobaths in gray. ACC – Alaska Coastal Current; BSC – Bering Slope Current.

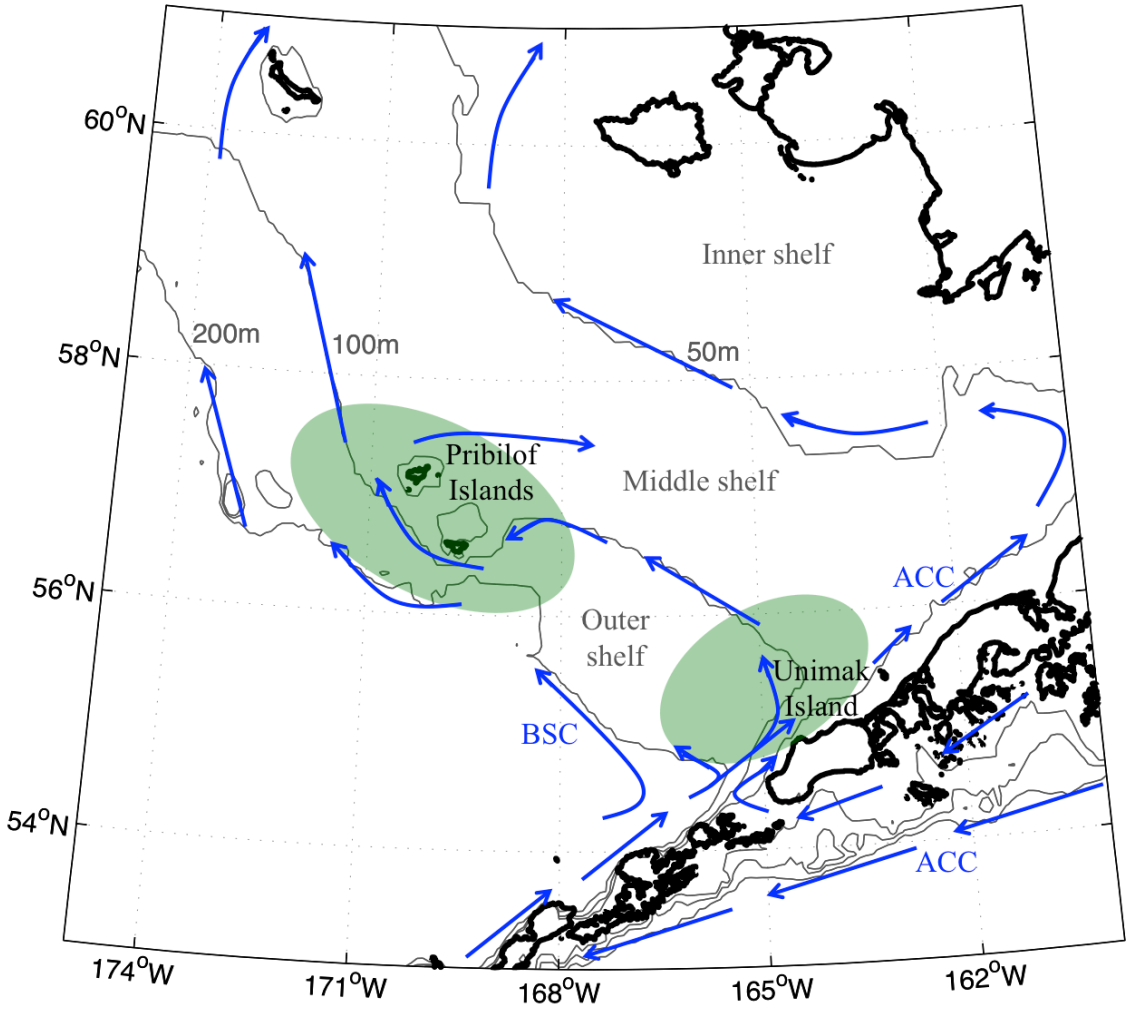

Figure 2. (a) Temperature-dependent egg development time. (b) Temperature-dependent growth rates of yolksac and feeding (preflexion and late) larvae; growth rate is independent of size. (c) Length of larvae with age-dependent ("age", solid line) and temperature-dependent (dotted and dashed lines) growth rates given constant temperature.

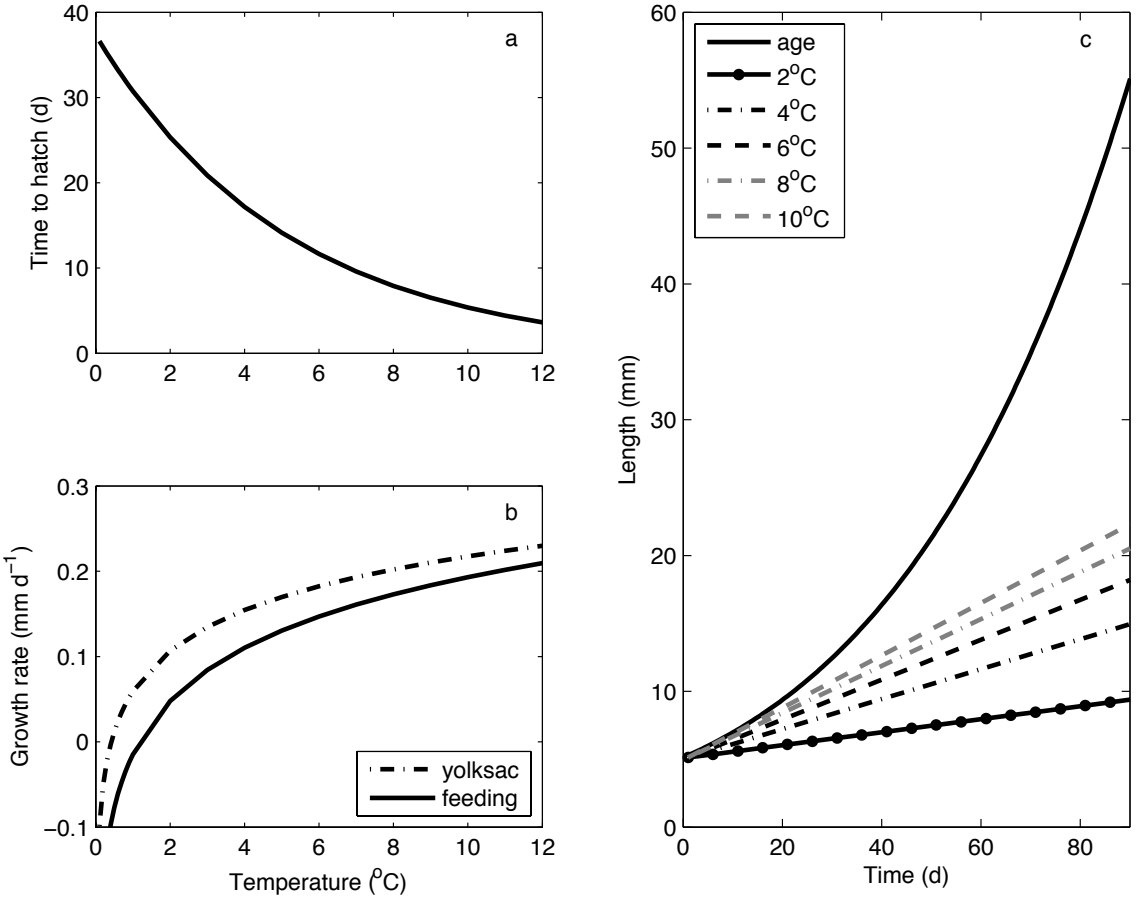

Figure 3. Spawning initial locations released on the dates shown. Light grey = Cold Contracted; Dark grey = Transport; Black = Warm Expanded. Polygons are overlapping and all share the same western and southern boundaries.

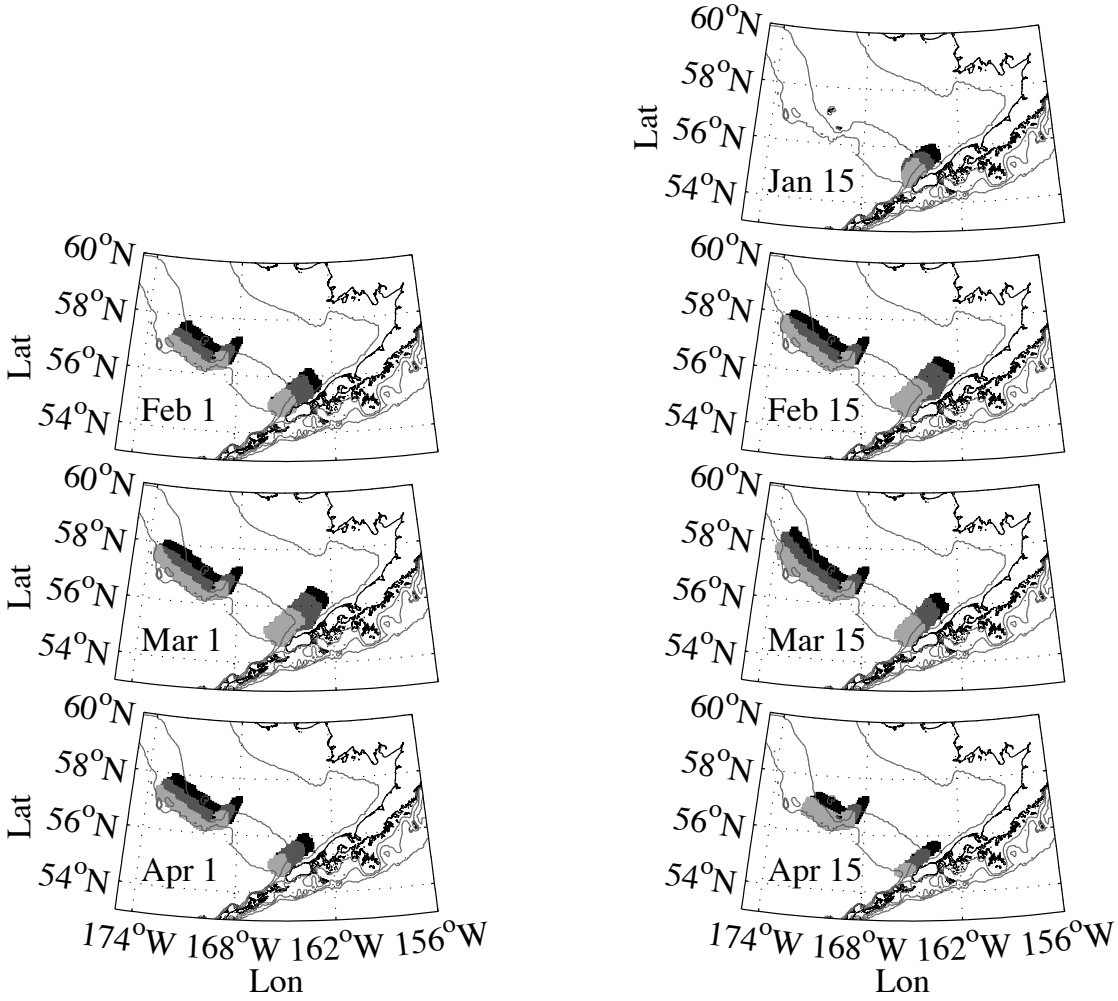

Figure 4. Depth distribution of early life stages from observations (black) compared to the model parameterization with the highest skill in reproducing horizontal distributions (grey). This model had temperature-based growth and vertical behavior 2 – passive eggs and yolksac larvae, and preflexion and late larvae that move to the middle of the mixed layer. Depth distribution is presented as a histogram of the weighted mean depth of each MOCNESS tow (observations) or each day (model).

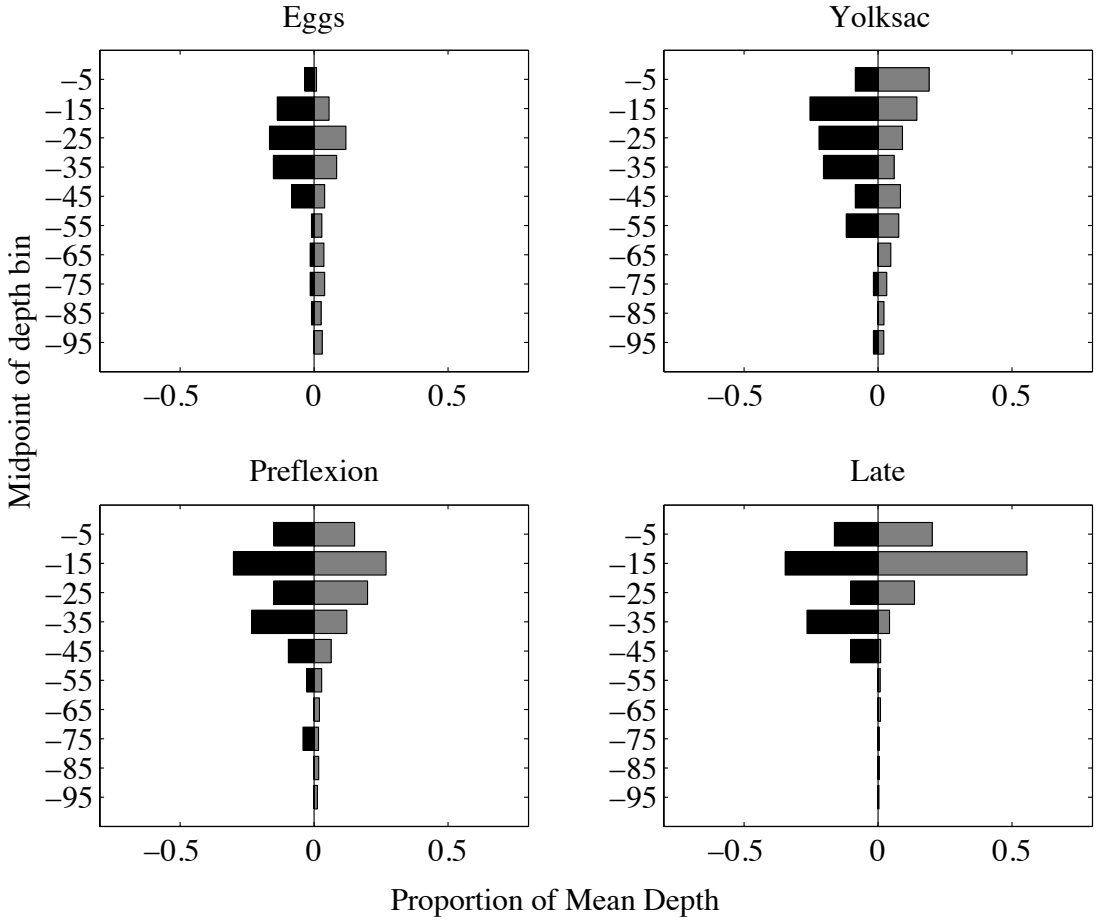

Figure 5. Contour plots of the relative concentration of early life stages in cold year (1995, 1997, 1999, 2000, 2006-2012) simulations. Relative concentration was calculated as the fraction of the mean number of particles found in each grid cell with observations. 40 d Late = spawning times delayed by 40 d; Transport Only = same times and locations of spawning in cold and warm years; Contracted = spawning locations contracted to the southwest.

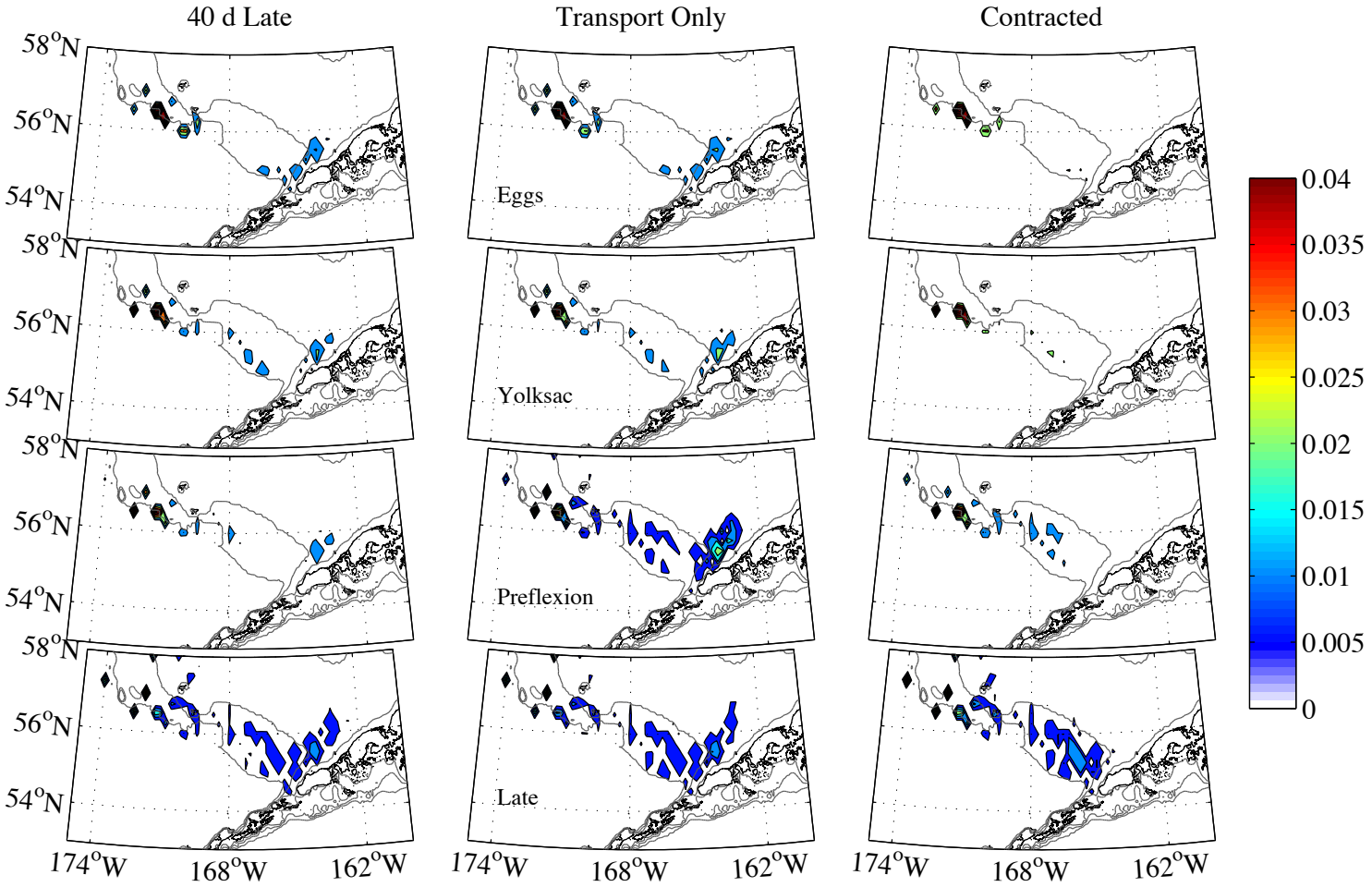

Figure 6. Contour plots of the relative concentration of early life stages in warm year (1996, 2002, 2003, 2005) simulations. Relative concentration was calculated as the fraction of the mean number of particles found in each grid cell with observations. 40 d Early = spawning times advanced by 40 d; Transport Only = same times and locations of spawning in cold and warm years; Expanded = spawning locations expanded to the northeast.

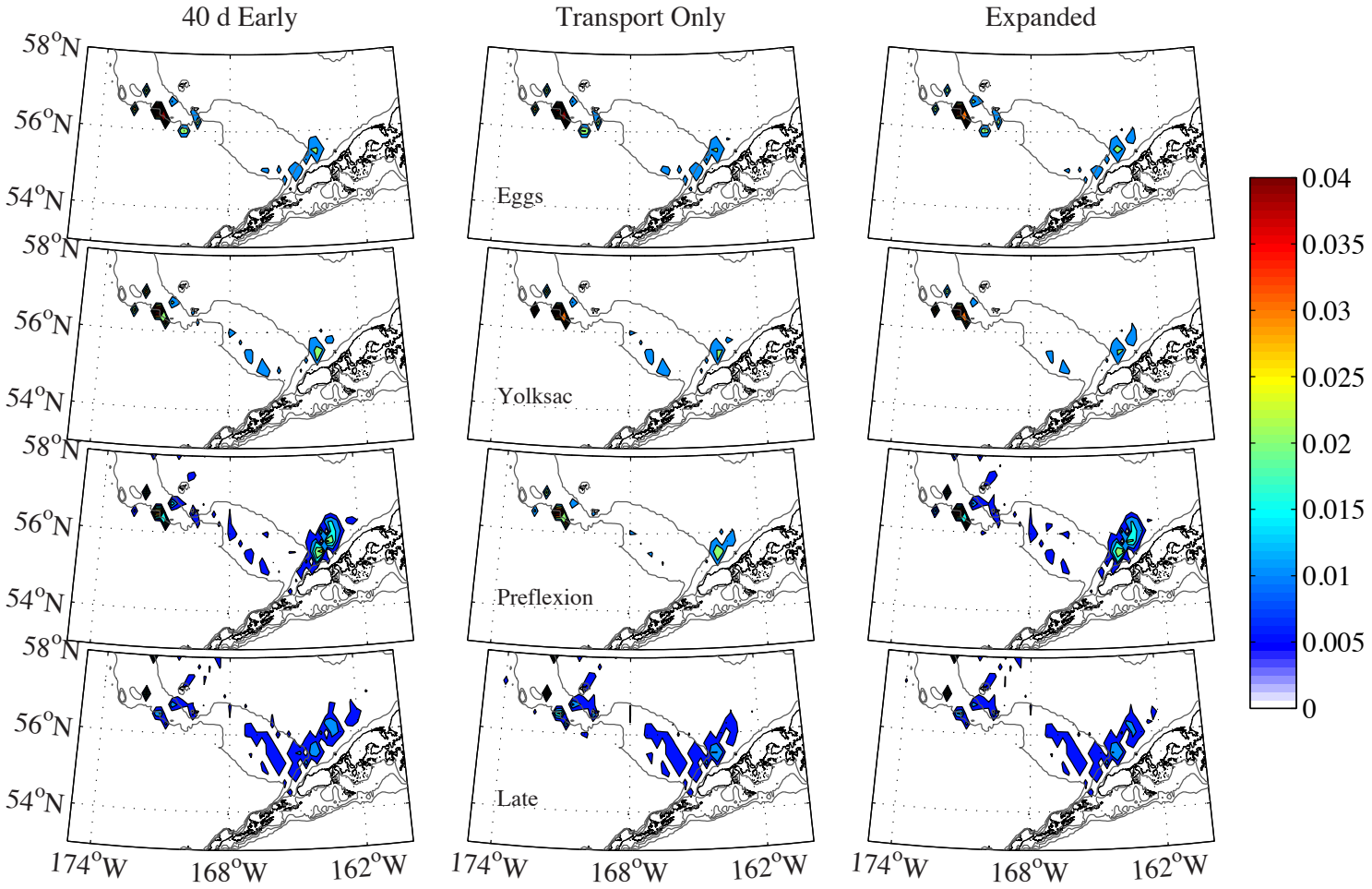

Figure 7. Observed (circles) and simulated Contracted (triangles) centers of gravity, major axes, and minor axes for the distributions of different pollock early life stages in cold (blue; 1995, 1997, 1999, 2000, 2006-2012) and warm (red; 1996, 2002, 2003, 2005) years.

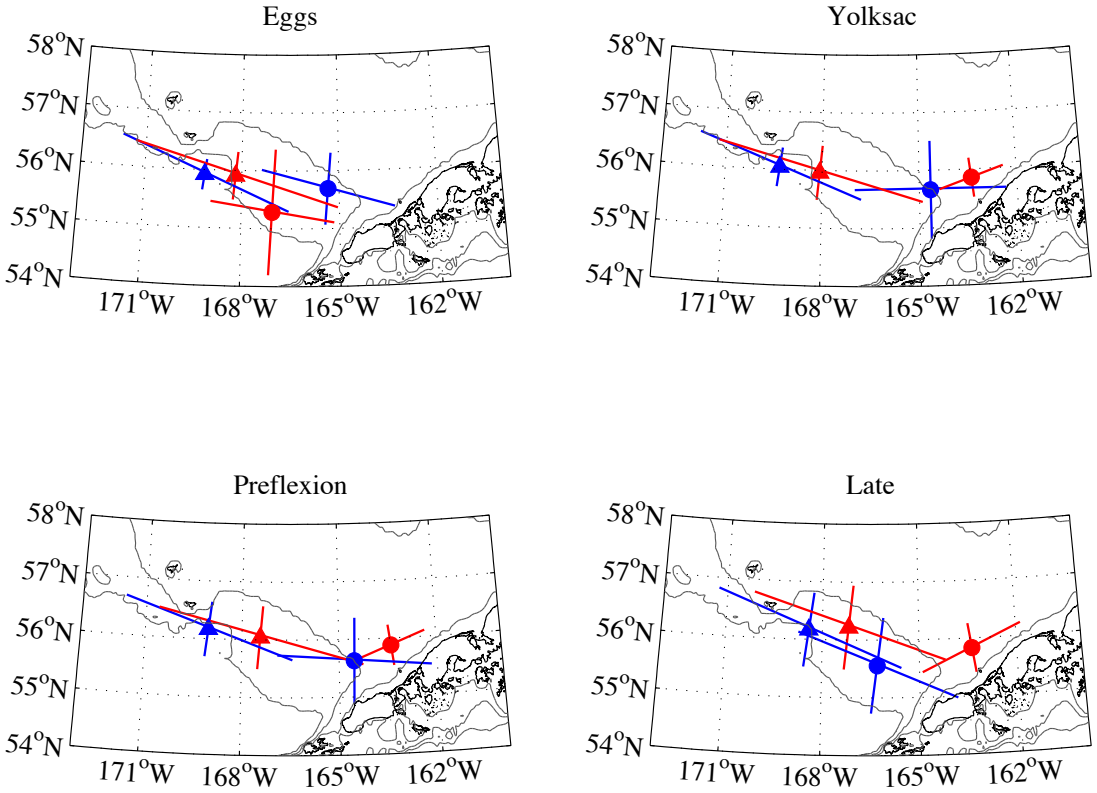

Figure 8. Mean standard length (mm) of all larvae by date in the Transport Only simulations for cold (black line; 1995, 1997, 1999, 2000, 2006-2012) and warm (grey line; 1996, 2002, 2003, 2005) years. Standard length (mm) of larval and juvenile pollock from observations in 2008-2010 (dots).